POLARIS is a copper-binding peptide required for ethylene signalling control in *Arabidopsis*

Authors

Anna J. Mudge[1†], Saher Mehdi[1†‡], Will Michaels[1,2†], Beatriz Orosa-Puente[1‡‡], Weiran Shen[1], Charlie Tomlinson[2‡‡‡], Wenbin Wei[1], Claudia Hoppen[3], Buket Uzun[3], Dipan Roy[1], Flora M. Hetherington[1‡‡‡‡], Jennifer F. Topping[1], Ari Sadanandom[1], Georg Groth[3], Nigel J. Robinson[1,2*], Keith Lindsey[1*]

Affiliations

[1]*Department of Biosciences, Durham University, Durham, UK*

[2]*Department of Chemistry, Durham University, Durham, UK*

[3]*Institute of Biochemical Plant Physiology, Heinrich Heine University Düsseldorf, D-40204 Düsseldorf, Germany*

[†]These authors contributed equally to this work

[‡]Present address: wellOwise Research and Development, IIITD Innovation & Incubation Centre, New Delhi, Delhi - 110020, India.

[‡‡]Present address: School of Biological Sciences, University of Edinburgh, Edinburgh EH9 3FF, UK; and Centro Singular de Investigación en Química Biolóxica e Materiais Moleculares (CIQUS) and Departamento de Química Orgánica, 15782, Universidade de Santiago de Compostela, Spain

[‡‡‡]Present address: Department of Biology, University of York, Heslington, York YO10 5DD, U.K.

[‡‡‡‡]Present address: University of Bath, Claverton Down, Bath BA2 7AY, U.K.

*Joint corresponding authors: keith.lindsey@durham.ac.uk; nigel.robinson@durham.ac.uk

Running title: The POLARIS peptide regulates ethylene responses

ABSTRACT

Ethylene signalling represents one of the classic hormonal pathways in plants, with diverse roles in development and stress responses. The dimeric ethylene receptor localizes to the endoplasmic reticulum (ER) and contains Cu(I) ions essential for ethylene binding and signal transduction. The final steps of Cu(I) incorporation into the ethylene receptor, and its link with receptor conformation are ill-defined. We previously discovered that mutants in the *Arabidopsis* gene *POLARIS* (*PLS*), encoding a 36 amino acid peptide, exhibit enhanced ethylene signalling responses, suggestive of reduced receptor activity. Here we report PLS binds copper as a 1:2 thiol-dependent Cu(I):PLS_2 complex, with an affinity of 3.79 (±1.5) x10^{19} M^{-2}. We demonstrate that PLS localizes to endomembranes and interacts with the transmembrane domain of receptor protein ETR1, the Cu(I) chaperones ATX1 and CCH, and Cu(I)-transporting P_{1B}-type ATPase RAN1. *PLS* transcription is up-regulated by auxin and down-regulated by ethylene, and so PLS-cuproprotein interactions provide mechanisms to modulate the activity of ETR1 to regulate ethylene responses in high auxin tissues.

Keywords: Plant hormone signalling, Arabidopsis, Ethylene, Protein metallation, Receptor

53 **INTRODUCTION**

54 Ethylene is used by plants as a gaseous hormone to regulate many aspects of
55 development and responses to biotic and abiotic stresses (Johnson and Ecker, 1998).
56 It is perceived by a family of receptors that, in *Arabidopsis*, comprises 5 members, ETR1
57 (ETHYLENE RESPONSE 1), ERS1 (ETHYLENE RESPONSE SENSOR 1), ERS2,
58 ETR2, and EIN4 (ETHYLENE-INSENSITIVE 4) (Chang et al, 1993; Hua et al., 1995,
59 1998; Sakai et al., 1998) located on the endoplasmic reticulum (ER) (Chen et al., 2002;
60 Grefen et al., 2008). The receptors are related to bacterial two-component systems
61 (Chen et al., 2002), form dimers through disulphide bonding at the N-terminal
62 hydrophobic domains (Schaller et al., 1995; Hall et al., 2000) and contain Cu(I) ions
63 bound to residues Cys65 and His69, essential for ethylene binding and signal
64 transduction (Rodriguez et al., 1999; McDaniel and Binder, 2012). In the absence of
65 ethylene these receptors activate a negative regulator CTR1 (CONSTITUTIVE TRIPLE
66 RESPONSE 1), which is a mitogen-activated protein kinase kinase kinase (MAPKKK),
67 so preventing ethylene responses (Chang, 2003; Gao et al., 2003). Mechanisms by
68 which receptor activity is regulated are not fully understood.

69 Introduction of copper to the ER and ethylene receptor requires the RAN1
70 (RESPONSIVE TO ANTAGONIST1) protein. This is a predicted copper-transporting P-
71 type ATPase homologous to the yeast Ccc2p and to human Menkes and Wilson disease
72 proteins (Hirayama et al., 1999). Strong loss-of-function mutants of *RAN1* in *Arabidopsis*
73 (e.g. *ran1-3*, *ran1-4*) exhibit an enhanced ethylene signalling response (Binder et al.,
74 2010), consistent with a loss of receptor function, and similar to higher order loss-of-
75 function receptor mutants, which also show an ethylene hypersignalling phenotype (Qu
76 et al., 2007). Mechanisms of copper homeostasis at ETR1 are unknown, as is true for
77 other compartmentalized cuproproteins supplied with copper, for example via Ccc2p,
78 Menkes or Wilson ATPases. RAN1 in Arabidopsis localizes to endomembrane systems,
79 including *trans*-Golgi and ER compartments, and is necessary for both the biogenesis
80 of ethylene receptors and copper homeostasis - loss of function *ran1* mutants suggest
81 copper is required for both ethylene binding and receptor function (Binder et al., 2010).
82 RAN1 can interact directly with ETR1 and the copper chaperones ANTIOXIDANT1
83 (ATX1) and COPPER CHAPERONE (CCH), suggestive of a transfer of copper between
84 proteins to deliver it to the ethylene receptor as part of the receptor biogenesis pathway

85 at the ER (Hoppen et al., 2019).

86 Our understanding of copper homeostasis at the receptor is still incomplete,
87 however. For example, how is Cu(I) delivery from RAN1 to ETR1 mediated? Are there
88 other Cu(I)-binding components involved? Is metalation of the receptor regulated in a
89 tissue-specific way or in response to the hormonal environment in a tissue? Is this
90 process part of the crosstalk mechanism with other hormone signaling pathways? It is
91 well established that ethylene signaling interacts with and is impacted by other hormonal
92 pathways but does this influence the receptor metalation state and with developmental
93 consequences? In this paper we show that a peptide, POLARIS, binds copper and is
94 linked to both the copper trafficking pathway and ETR1-mediated ethylene signalling.
95 We show POLARIS is unlikely to act as a metallochaperone intermediary but may form
96 copper-adducts with ETR1 and/or its metalation partners. We suggest this provides cell
97 type control and a crosstalk regulatory mechanism for ethylene responses through a
98 role in its physical interaction with the ethylene receptor.

99

100 # RESULTS

101 **The POLARIS peptide is a negative regulator of ethylene responses**

102 The *POLARIS* gene of *Arabidopsis* (AT4G39403) encodes a 36 amino acids peptide
103 (Figure 1A) translated from a low-abundance transcript that, in light-grown seedlings, is
104 most strongly expressed in the embryo and silique, seedling root tip and leaf vascular
105 tissues (Figure S1), a pattern reflected in promoter-reporter expression patterns
106 (Casson et al., 2002). We have previously shown that the loss-of-function *pls* mutant
107 has some phenotypic similarities to *ran1* loss-of-function alleles and to *ctr1*, exhibiting a
108 triple response phenotype (short hypocotyl and root, exaggerated apical hook, radial
109 expansion) in the dark in the absence of ethylene (Chilley et al., 2006), and a short root
110 in light-grown seedlings, consistent with its expression in the root meristem in light-
111 grown seedlings (Figure 1B). Transgenic complementation of the mutant by the *PLS*
112 gene suppresses the mutant phenotype (Casson et al., 2002). The *pls* mutant
113 phenotype is rescued by the gain-of-function ethylene resistant mutation *etr1-1* and
114 pharmacological inhibition of ethylene signalling by silver ions (Chilley et al., 2006).
115 Ethylene gas production in the *pls* mutant is at wild type levels, indicating the peptide
116 may play a role in ethylene signalling rather than biosynthesis (Chilley et al., 2006). *PLS*

117 transgenic overexpressers (PLSOx seedlings) in contrast exhibit a suppression of the
118 triple response phenotype when grown in the presence of the ethylene precursor ACC,
119 similar to the gain of function *etr1-1* mutant, but this suppression is incomplete (PLSOx
120 seedlings show some response to ACC; Casson et al., 2002; Chilley et al., 2006).
121 PLSOx also partially suppress the *ctr1* mutant phenotype, indicating that the PLS
122 peptide acts upstream of CTR1 (Chilley et al., 2006).

123 To further investigate the *pls* molecular phenotype, we carried out an RNA-seq
124 analysis on loss-of-function *pls* mutant and PLSOx transgenic overexpressor seedlings
125 to identify differentially regulated genes, with mutant and overexpressor each compared
126 with wild type seedlings of the same ecotype as controls. The *pls* mutant expresses no
127 full length PLS coding sequence due to a T-DNA insertion in the coding region of *PLS*
128 and disrupting function (Casson et al., 2002), while the PLSOx seedlings express
129 significantly higher levels of *PLS* transcript compared to wild type ($\log_2$ fold 10.8, *padj*
130 value = 2.02×10^{-33}; Tables S1, S2). 836 genes were significantly up-regulated and 292
131 down-regulated in the *pls* mutant compared to wild type control seedlings (padj value <
132 0.05) (Table S1). 1487 genes were significantly up-regulated and 1281 down-regulated
133 in PLSOx seedlings compared to wild type (padj value < 0.05; Table S2). Gene Ontology
134 (GO) analysis of genes upregulated in *pls* mutant seedlings compared to wild type
135 showed significant enrichment of genes associated with responses to hormone
136 signalling, biotic and abiotic defence responses, and cell death (Table S3; Figure S2A).
137 Out of 307 GO:0009723 (response to ethylene) genes, 25 were significantly up-
138 regulated and 7 down-regulated in the *pls* mutant compared with the wild type, with 40
139 up-regulated and 18 down-regulated in the PLSOx seedlings (Figure 1C; Table S3, S4,
140 S5 and S6; Mudge et al., 2024), indicating a requirement for control over *PLS* expression
141 levels for correct ethylene responses. While GO:0009723 (response to ethylene) is
142 significantly enriched in genes up-regulated in the *pls* mutant compared to wild type
143 (*FDR = 0.00062*; Table S3), a large number of up-regulated genes in *pls* are significantly
144 associated with immunity, response to pathogens and hypersensitive response (Table
145 S3 and Figure S2A). Down-regulated genes in *pls* were significantly enriched in GO
146 categories of hormone biosynthetic processes (GO:0042446, *FDR = 0.038*), hormone
147 metabolic process (GO:0042445, *FDR = 0.0096*) and regulation of hormone levels
148 (GO:0010817, *FDR = 0.0013*) (Table S4, Figure S2B; Mudge et al., 2024), consistent

149 with our previous studies that described PLS-dependent crosstalk between ethylene,
150 auxin and cytokinin signalling (Liu et al., 2010, 2013; Moore et al., 2015). In PLSOx
151 overexpressors, both up- and down-regulated genes similarly included those associated
152 with GO terms hormone response, stress response and immune response, and genes
153 associated with photosynthesis are downregulated in PLSOx seedlings, consistent with
154 repressed photosynthetic activity in root tips (Table S5 and S6, Figure S2C, D; Casson
155 et al., 2002). These data are consistent with a role for PLS in a number of ethylene
156 responses and other related signalling, stress and developmental processes.

157 To understand better the relationship between PLS peptide structure and
158 function between species, we carried out hydroponic feeding experiments using
159 synthetic versions of PLS peptide from both *Arabidopsis* and its close relative *Camelina*
160 *sativa*. *C. sativa* contains a gene with partial sequence identity to the *Arabidopsis PLS*
161 gene, encoding a predicted peptide sequence that is 22 amino acids long and identical
162 to the N-terminal 22 amino acids of the *Arabidopsis* PLS except for a phenylalanine to
163 serine substitution at position nine (Figure 1A). We synthesized full-length PLS peptide,
164 PLS(FL) and truncated versions from both *Arabidopsis* and *C. sativa* (Figure 1A) and
165 supplied the peptides to *Arabidopsis pls* mutant seedlings hydroponically. The full-length
166 peptides from both *Arabidopsis* and *C. sativa* and the N-terminal 22 amino acids
167 sequence of the *Arabidopsis* peptide (N1) were each able to rescue the short primary
168 root length of the *Arabidopsis pls* mutant (Figure 1D), similar to transgenic
169 overexpression and genetic complementation using the wild type *PLS* coding sequence
170 (Casson et al., 2002; Chilley et al., 2006). The mean primary root length of wild type
171 (C24) seedlings did not change across all peptide treatments, while supply of *pls*
172 seedlings with 50 nM PLS(FL) and N1 peptides showed a rescue of root growth (Figure
173 1E), and *t*-tests showed there was no significant difference between the rescue effects
174 of PLS(FL) and PLS(N1); $P > 0.1$, n = 25). However, neither a 9 amino acids sequence
175 (N2, Figure 1E) from the N-terminus, nor C-terminal sequences of 14 (C1) or 24 (C2)
176 amino acids from *Arabidopsis* PLS were able to rescue the mutant (Figure 1E); each of
177 these shorter peptides lacks one of the two Cys residues found in the functional longer
178 length peptides PLS(FL) and PLS(N1). A fluorescent tagged (5-carboxyfluorescein, 5-
179 FAM) version of the *Arabidopsis* N-terminal 22 amino acids sequence of the peptide
180 (N1) is taken up by the roots, and also rescues the mutant root phenotype (Figures S3A,

181 B).

182

183 **PLS localizes to endomembranes including the endoplasmic reticulum**

184 Since genetic studies suggest that PLS acts close to the ethylene receptor (*18*), we
185 hypothesized that it should localize to the same subcellular compartment as ETR1. The
186 ethylene receptor in *Arabidopsis* is localized predominantly to the ER (Chang, 2003),
187 and a *proPLS::PLS:GFP*-generated fusion protein (PLS:GFP) was used to investigate
188 sub-cellular localization. Of five independent transformants with a single-copy insertion
189 of the *proPLS::PLS:GFP* gene in a *pls* mutant background, four were found to
190 complement fully the *pls* mutant (Figure S4), similar to the wild type cDNA (Casson et
191 al., 2002), demonstrating functionality of the gene fusion. The PLS:GFP was found to
192 co-localize in transgenic plants with the ER marker dye ER-Tracker red™, which binds
193 sulphonylurea receptors of ATP-sensitive channels on the ER (Thermofisher; Figures
194 2A-C). It also co-localizes with an ER lumen-targeted red fluorescent protein RFP-HDEL
195 (Lee et al., 2013) (Figures 2G-I). These observations suggest PLS:GFP locates both on
196 the ER membrane and in the lumen. PLS:GFP also appears to localize to the nucleus
197 and cytoplasm (Figure 2). As controls, free GFP protein expressed under the control of
198 the *PLS* promoter is not co-localized to the ER (Figures 2D-F) and, as expected, the
199 Golgi marker SH:GFP does not co-localize with ER Tracker (Figures 2M-O). *Trans*-
200 Golgi-localized SULFOTRANSFERASE1 (ST1) mCherry (Bauer and Papenbrock,
201 2002) visualization shows PLS:GFP does not localize to the Golgi (Figures 2J-L). To
202 further clarify the side of the ER membrane on which PLS localizes, transient expression
203 of redox-sensitive GFP (roGFP2) fusions of PLS were carried out. The different
204 excitation properties of roGFP2 in an oxidizing (ER lumen) or reducing environment
205 (cytosol) allows discrimination of the precise location of PLS fused to RoGFP2.
206 Ratiometric analysis and comparison with proteins of known localization (i.e. cytosolic
207 RoGFP2, ER luminal RoGFP2, cytosolic v-SNARE SEC22-GFP, ER luminal RoGFP2-
208 SEC22; *26*) revealed that PLS as either an N- or C-terminal roGFP2 fusion resides at
209 the cytosolic side of the ER (as well as to other vesicular compartments; Figure 2P).
210 However, there may be some translocation of PLS:GFP into the ER lumen as indicated
211 by co-localization with RFP:HDEL.

212

213 **PLS interacts with the ethylene receptor protein ETR1**

214 We hypothesized that PLS plays a role in receptor function and investigated whether
215 this involved direct interaction with the receptor complex. Preliminary experiments using
216 yeast 2-hybrid analysis suggested that PLS interacts with ETR1 (Figure S5).
217 Confirmation of the physical interaction between PLS and ETR1 in plants came from co-
218 immunoprecipitation (Co-IP) analysis. *Agrobacterium* containing a plasmid encoding
219 PLS linked to a C-terminal GFP and ETR1 with a C-terminal HA tag was infiltrated into
220 *Nicotiana benthamiana* leaves for transient expression. After 3 d, interaction was
221 confirmed by western blotting after Co-IP with either anti-GFP beads (showing PLS pulls
222 down ETR1) or anti-HA beads (showing ETR1 pulls down PLS) (Figure 3A). GFP-only
223 controls did not show binding with ETR1, demonstrating the interaction is dependent on
224 the presence of the PLS peptide. The addition of 0.5 μM copper sulphate to the protein
225 extract used for Co-IP experiments stabilized the PLS-ETR1 interaction. The presence
226 of copper ions resulted in almost 3-fold more PLS:GFP detected upon pulldowns with
227 ETR1-HA, or conversely of ETR1-HA pulled down with PLS-GFP, compared to the same
228 assay in the presence of the metal chelator 2 mM EDTA (Figures 3A, B).

229 To investigate the specificity of PLS binding, synthetic full length PLS peptide
230 PLS(FL) was introduced into infiltrated *N. benthamiana* leaves 30 min before tissue
231 harvest in the presence of both copper to maximise PLS-ETR1 interaction and the
232 proteasome inhibitor MG-132 to prevent protein degradation. The addition of 25 nM
233 synthetic PLS caused a ca. 80% reduction in PLS-GFP binding to ETR1-HA (Figures
234 3C, D), suggesting that the synthetic PLS peptide competes for ETR1 binding, showing
235 the specificity of PLS for ETR1. The anti-GFP beads bound two sizes of PLS-GFP
236 protein (Figure 3E), both of which were larger than a GFP-only control, suggesting that
237 the PLS peptide undergoes cleavage, a change in conformation, post-translational
238 modification or incomplete reduction of Cys residues on some PLS. When using ETR1-
239 HA to pull down PLS-GFP, only the larger peptide was present (Figures 3E, F),
240 suggesting that ETR1 binds a longer version of the PLS peptide.

241 To pinpoint the interaction site at the receptor in more detail, *in vitro* binding
242 studies were performed with purified receptor variants and PLS by microscale
243 thermophoresis (MST; Figure 3G). Binding of PLS was observed only with receptor
244 variants containing the N-terminal transmembrane domain (TMD). In contrast, no

245 binding was detected with ETR1 lacking this domain ($ETR1^{306-738}$). The TMD harbors
246 the ethylene and copper binding region (Schott-Verdugo et al., 2019).
247
248 **PLS binds Cu(I) and forms protein-protein interactions with copper chaperones**
249 **ATX and CCH and with RAN1**
250 Cysteine residues are common metal-ligand binding residues in low molecular weight
251 copper-handling peptides, and predictions of PLS structure suggests a single a-helix
252 plus unstructured region with two cysteines ($CX_{10}C$ arrangement where X is any amino
253 acid), with some analogy to copper-metallochaperones such as Cox17 or other CX_9C
254 twin proteins (Robinson and Winge, 2010). In view of both structural considerations and
255 the copper-dependency of ETR1 we determined whether the two cysteine residues (C6
256 and C17) in PLS play a functional role, by analysing both *pls* mutant complementation
257 and in copper binding by PLS variants. A mutated *Arabidopsis* full-length peptide in
258 which both cysteines were replaced with serines, PLS(FL C6S, C17S), was non-
259 functional in hydroponic root feeding assays, failing to rescue the short primary root
260 phenotype of the *pls* mutant (Figure 4A). Furthermore, as indicated above, the 9 amino
261 acids sequence N2 and C-terminal sequences C1 and C2 from *Arabidopsis* PLS, which
262 each contain only one cysteine residue, were unable to rescue the mutant (Figure 1E).
263 These results indicate the requirement of the two cysteine residues for biological activity,
264 measured as primary root growth. Interestingly, RNA-seq data showed that nineteen out
265 of 287 genes associated with response to metal ion (GO:0010038) were also
266 significantly down-regulated in the *pls* mutant (Table S4, Figure S2B, enrichment *FDR*
267 *= 0.000057*; *20*).
268 To determine a possible role for PLS and the cysteine residues in binding Cu(I),
269 synthesised PLS peptide was titrated with Cu(I) ions under strictly anaerobic conditions
270 and monitored for copper-dependent spectral features (Figures 4B-D). Both UV-vis
271 (putative metal-to-ligand charge-transfer) and fluorescence (putative tyrosine solvent
272 access) spectra of PLS changed as a function of Cu(I) ion concentration, consistent with
273 complex-formation (Figure 4C). We titrated PLS peptide against bicinchoninic acid (BCA;
274 Figure 4B), which is a chromophore that binds Cu(I) (Xiao et al., 2011; Figures 4D and
275 S6). The rationale was to determine whether PLS could compete Cu(I) from BCA,
276 indicative of binding by PLS. PLS peptide was titrated with Cu(I) in the presence of 87 μM

277 BCA. PLS peptide (44.8 μM) increased the concentration of Cu(I) required to saturate
278 BCA increased by ca. 20 μM (Figure 4B), and the initial gradient is shallower than in the
279 control of BCA and Cu(I) but lacking PLS. Thus PLS withholds Cu(I) from BCA, implying
280 an affinity for Cu(I) (K_{Cu} PLS) tighter than K_{Cu} of BCA, and these data also provide support
281 for a 2:1 stoichiometry of binding to the tightest site. Titration experiments also show that
282 although synthetic PLS(FL) withholds Cu(I) from BCA (Figure S7), a mutant PLS (FL C6S,
283 C17S) does not (Fig. S8), confirming a role for those cysteine residues in Cu(I) binding.
284 As an additional and complementary strategy, to eliminate potential solubility problems of
285 PLS in determining accurately the stoichiometry and affinity for Cu(I) (these studies
286 require complete solubility for precise affinity quantification), we also tested a PLS fusion
287 to maltose binding protein (MBP-PLS) which was found to retain solubility when titrated
288 with Cu(I) ions under strictly anaerobic conditions. MBP-PLS (14 μM) was found to
289 withhold ca. 7 μM Cu(I) from BCA, again indicative of a 2:1 PLS:Cu(I) stoichiometry, and
290 tight binding is cysteine-dependent (Figure 4E). A β_2 affinity of 3.79 (±1.5) x10^{19} M^{-2} was
291 determined by competition against an excess of BCA, and the fit significantly departs from
292 simulations 10x tighter or weaker (Figures 4F, S9).

293 Metal binding in biology is challenging to predict because the formation of metal-
294 protein complexes is a combined function of metal affinity for a given protein and metal
295 availability, which would need to be known for Cu(I) in the *Arabidopsis* cytosol in the
296 case of PLS (assuming the same orientation of binding residues as with the GFP tag;
297 Figure 2P). Cu(I) occupancy of the cytosolic copper chaperone ANTIOXIDANT
298 PROTEIN 1 (ATX1) tracks with fluctuations in available cytosolic Cu(I) such that its
299 affinity approximates to the mid-point of the range of Cu(I) availabilities within this
300 eukaryotic compartment (Yu et al., 2017; Morgan et al., 2019). *Arabidopsis* ATX1 was
301 therefore expressed and purified to determine a 1:1 ATX1:Cu(I) stoichiometry and
302 affinity $K_{D\ Cu(I)}$ of 5.47 (±0.6) x10^{-18} M (Figure 4G inset, Figure S10). Figure 4F reveals
303 that the cytosolic concentration of PLS would need to exceed (improbable) millimolar
304 concentrations for Cu(I)-dependent homodimers to form at this cytosolic Cu(I)
305 availability (mathematical models and equations shown in Supplementary text). It is thus
306 unlikely that the Cu(I):PLS_2 complex alone delivers Cu(I) to, or retrieves it from, the
307 interacting cuproprotein ETR1. Cu(I)-dependent PLS heterodimeric complexes are the
308 more likely functional species.

309 To investigate possible interaction between PLS and Cu(I) transporter RAN1,
310 PLS was titrated against fluorescently labelled RAN1 and RAN1 truncation mutants for
311 comparison. RAN1, NterRAN1 and CterRAN1 (DeltaRAN1 in Figure 4H) were purified
312 and labelled as described (Hoppen et al., 2019). NterRAN1 is a truncation containing
313 only the two N-terminal metal-binding-domains, whereas CterRAN1 is a construct
314 lacking this region. Using MST, direct interaction was observed between PLS and
315 RAN1. Dissociation constants indicate that PLS interacts predominantly with the N-
316 terminal metal-binding-domains, but only weakly with the C-terminal region (Figure 4H).
317 Moreover, the soluble copper chaperones ATX1 and CCH also interact with PLS.
318 Titration experiments were carried out with fluorescently labelled copper chaperones
319 ATX1, CCH and CCHΔ, a mutant lacking the plant specific C-terminal extension; though
320 the C-terminus on its own (DeltaN) is not soluble and can thus not be checked for
321 interaction with PLS. PLS interacts with these soluble copper chaperones at similar
322 affinity as obtained for RAN1 (Figure 4I). Of relevance here is the observation that ATX1
323 interacts directly with RAN1 to deliver copper at the ER (Li et al., 2017).
324

325 **DISCUSSION**

326 We present evidence of a role for the PLS peptide as a new Cu(I)-binding peptide that,
327 based on its physical interactions with the receptor and other Cu(I) delivery proteins,
328 and its ethylene signalling function as determined by genetic and physiological
329 experiments, acts as a regulatory component of the ethylene signalling pathway.
330 Peptides can act as ligands for receptor kinases to regulate signalling pathways, such
331 as in plant immunity (Campos et al., 2018), development (Willoughby and Nimchuk,
332 2021) or in response to abiotic stresses (Kim et al., 2021). We propose that the PLS
333 peptide is a new component of the regulatory mechanism for ethylene receptor function
334 linked to its copper-binding activity (Rodriguez et al., 1999). Loss of copper binding
335 through mutation of the two cysteines in PLS ablates its biological activity (Figures 1D,
336 E, S8). The *pls* mutant phenotype has some similarities (enhanced ethylene responses)
337 to strong *ran1* mutant alleles in which copper delivery to the receptor is compromised
338 (Binder et al., 2010), and shares (statistically significant) overlap in DEGs with the *ctr1*
339 mutant, whereby 11.9% of the *ctr1* DEGs are shared with *pls* (each compared to the
340 respective wild types; Figure S11).

341 Many plant peptides involved in signalling are processed from longer pre-
342 proteins (Olsson et al., 2019). In contrast, PLS is translated from an open reading frame
343 to produce a functional 36 amino acids peptide; the peptide appears to be cleaved or
344 otherwise modified in the cell (Figure 3E). It is possible that the three arginines (amino
345 acids 10-12) may represent a cleavage site (Duckert et al., 2004; Capraro et al., 2015)
346 which would produce the observed shorter GFP fusion protein (ca. 30 kD) detected in
347 anti-GFP co-IP blots (Fig. 3E). The size of this PLS-GFP cleavage product suggests that
348 this peptide fragment represents GFP (ca. 27 kDa) plus a 3 kDa fragment of the C-
349 terminal region of PLS. Such cleavage would likely inactivate PLS function as we
350 demonstrate that shorter N- and C-terminal fragments (each with only one cysteine
351 residue) are not biologically active (Figure 1E). While PLS:GFP localizes to several
352 subcellular compartments (though not the *trans*-Golgi), some localizes to the ER where
353 the ethylene receptor is found (Figure 2). Furthermore PLS can interact directly with the
354 receptor protein ETR1 (and specifically with the N-terminal copper-binding
355 transmembrane domain of ETR1); with the Cu-transporting P-type ATPase RAN1; and
356 with two Cu chaperones, ATX1 and CCH.
357 Previously there has been proposed a model for copper delivery into the cell via
358 the COPT family of transporters, which are located at the root plasma membrane (Chen
359 et al., 2022), to RAN1 via ATX1 and/or CCH (Li et al., 2017; Hoppen et al., 2019).
360 Arabidopsis has three known copper chaperones, ATX1, CCH and a copper chaperone
361 for superoxide dismutase CCS (Casareno et al., 1998; Chu et al., 2005; Puig et al.,
362 2007). These are required for copper homeostasis, and both ATX1 and CCH have been
363 shown to interact with RAN1 (Li et al., 2017), providing a link with ethylene signalling
364 (Andrés-Colás et al., 2005; Puig et al., 2007). Chaperones are required for the transport
365 of reactive copper to the correct compartment via these chaperones, avoiding
366 cytotoxicity, following import into the cell; and into the xylem from the cytosol via HMA5,
367 which is structurally similar to RAN1 (Williams and Mills, 2005; Burkhead et al., 2009).
368 Loss of function mutants *cch* and *atx1* have no abnormal phenotype when grown under
369 standard conditions, but the *atx1* and the *atx1 cch* double mutant, though not the *cch*
370 single mutant, are hypersensitive to exogenous copper (Shin et al., 2012). ATX1 and
371 CCH functions have likely diverged, a view supported by their differential transcriptional
372 regulation by copper and different cell type specificities (Shin et al., 2012). The *ran1*

373 mutant is however not copper-hypersensitive, while *hma5* is; and the *pls* mutant is, like
374 *ran1*, not copper hypersensitive (Figure S12), indicative of a role that is distinct from that
375 of ATX1 or CCH. The ATX1 interaction with RAN1 is indicative of its role in copper
376 transport from the cell surface to internal targets, including RAN1 and potentially to or
377 from PLS.

378 A lack of copper delivery in the strong *ran1-3* and *ran1-4* null alleles causes
379 constitutive ethylene responses (Woeste and Kieber, 2000), producing a triple response
380 phenotype similar to the *pls* mutant (Casson et al., 2002). These *ran1* mutants fail to
381 bind ethylene due to the lack of copper at the ethylene binding site (Binder et al., 2010).
382 The decrease in ethylene binding in the *ran1-3* and *ran1-4* mutants is not due to reduced
383 levels of the ETR1 protein (Binder et al., 2010), and regulation of the ethylene receptor
384 ETR1 is generally regarded to be independent from *ETR1* transcription or degradation
385 (Hua et al., 1998). Weaker *ran1-1* and *ran1-2* alleles only show an ethylene response
386 phenotype if they are grown in the presence of copper chelators (Binder et al., 2010).
387 Therefore, defective RAN1 results in defective copper delivery to wild type receptors,
388 generating non-functional receptors which cannot interact with CTR1, resulting in
389 downstream ethylene responses.

390 Intriguingly, the *ran1-3* and *ran1-4* mutants with constitutive ethylene responses
391 are distinct from the ethylene insensitive *etr1-1* mutant, which also cannot bind copper.
392 Therefore, both the *etr1-1* mutant receptor and the strong *ran1* mutant alleles have
393 reduced ethylene binding capability but the *etr1-1* mutation, which is gain-of-function,
394 generates seedling phenotypes that are very different from seedlings carrying the
395 ethylene hypersensitive wild type receptors that simply lack copper due to defective
396 delivery (in *ran1-3* and *ran1-4).* A receptor carrying the *etr1-1* mutation is maintained in
397 its 'active' state and constitutively inhibits downstream ethylene responses, whilst in the
398 *ran1* mutants ETR1 remains in the 'inactive' state, promoting ethylene responses
399 (Binder et al., 2010). Those authors therefore proposed that copper has more than one
400 role in the regulation of ETR1 and ethylene signalling: it is crucial for binding ethylene
401 molecules but it is also needed for the process of signal transduction by the receptor
402 protein, by an unknown mechanism, to regulate downstream ethylene responses.

403 We propose that PLS represents a new component of this pathway, providing
404 some tissue-specificity to Cu(I) homeostasis at the ethylene receptor. Given the low

405 probability that PLS would act as a cytosolic copper chaperone directly, due to its
406 predicted low concentration in the cell and 2:1 stoiciometry (Figures 4F and G, S9 and
407 10), it more likely partners with other proteins for Cu(I) acquisition. The primary current
408 model for metallation of ETR1 is that Cu(I) is delivered to RAN1 by the chaperones ATX1
409 and/or CCH, then by RAN1 into the ER lumen; and then to ETR1 by a currently unknown
410 mechanism. Our data show that PLS interacts with cytosolic chaperones ATX1 and CCH,
411 and with RAN1 and ETR1. The RFP-HDEL and Rho-GFP co-localization experiments
412 indicate the presence of PLS in both the cytosol and ER lumen (as well as other
413 compartments; Figure 2).

414 Based on the evidence presented, we can consider three possible models for a
415 role for PLS in regulating ethylene responses based on its copper binding properties
416 (FIG. 5). In the first, a primary PLS function is in transferring Cu(I) from RAN1 to ETR1
417 in the ER lumen. In the second, PLS removes Cu(I) from the transmembrane domain of
418 ETR1. In the third, PLS interacts with ETR1 to modulate receptor conformation to
419 regulate its activity. Given that PLS interacts also with RAN1 and the chaperones, there
420 may exist a complex of these proteins at the ER to facilitate copper transfer and
421 homeostasis, but this has yet to be confirmed.

422 Since the *pls* mutant is rescued by the supply of silver ions (Casson et al., 2002),
423 and silver is likely delivered to the ethylene receptor via RAN1 (Binder et al., 2010), this
424 argues against Model 1 in which PLS acts downstream of RAN1 to metalate ETR1 in
425 the ER lumen. This would also be consistent with the data suggesting PLS is located
426 predominantly at the cytosolic side of the ER; but it binds to the transmembrane domain
427 of ETR1. It is also unlikely that PLS removes Cu(I) from the receptor (Model 2) as this
428 would inactivate the receptor and lead to enhanced ethylene signalling, which is the
429 opposite of what would be expected from the *pls* mutant phenotype. We therefore favour
430 Model 3 in which PLS binds ETR1 as part of the receptor biogenesis mechanism, with
431 the PLS-ETR1 physical interaction enhanced in the presence of copper (Fig. 3), to
432 regulate receptor conformation to generate the active form, in which ethylene responses
433 are repressed. This may be through regulation of Cu(I) homeostasis at the receptor, or
434 via other structural interactions - for example, PLS could physically block ethylene
435 binding at the Cu(I) pocket. This question can form the basis of future investigations. If
436 PLS is required for Cu(I) delivery, it may act redundantly with RAN1, accounting for the

437 relatively mild ethylene phenotype of the *pls* mutant (compared with e.g. *ctr1*).

438 Given that PLS is expressed in specific tissues, notably root tip and leaf vascular
439 tissue (Casson et al., 2002) it seems likely that PLS adds a level of regulation of receptor
440 function in specific tissues, with a focus in this paper on the root (though developmental
441 defects in the vascular patterning of the leaf are also observed in the *pls* mutant; Casson
442 et al., 2002). We propose that PLS acts to dampen ethylene responses at sites of high
443 auxin. *PLS* transcription is strongly up-regulated by auxin, and its expression profile is
444 similar to that of the auxin reporter DR5 (Sabatini et al., 1999; Casson et al., 2002). The
445 root tip, where *PLS* is most strongly expressed, is a site of high auxin concentration,
446 whereby an auxin maximum is formed around the stem cell niche to regulate both stem
447 cell identity and function (Sabatini et al., 1999). The vascular tissues are also a site of
448 high auxin (Bishopp et al., 2011). Auxin can induce ethylene biosynthesis by
449 upregulation of the ethylene biosynthetic enzyme ACC synthase (Abel et al., 1995), and
450 high ethylene concentrations can lead to both reduced meristem function and aberrant
451 division of the quiescent centre and cells within the stem cell niche and columella
452 (Ortega-Martinez et al., 2007). Therefore ethylene biosynthesis and signalling in the root
453 tip must be tightly regulated to allow growth control. *PLS* expression is transcriptionally
454 activated by auxin and suppressed by ethylene. We have shown in previous work that
455 there is crosstalk between PLS, ethylene and other signalling pathways, notably auxin,
456 cytokinin and ABA in the root (e.g. Liu et al., 2010, 2013; Moore et al., 2015), and the
457 distinctiveness of *pls* compared to other ethylene signaling mutants may be linked to its
458 restricted expression pattern. This network provides a mechanism to suppress growth-
459 inhibitory ethylene responses in the high auxin environment of the root tip, which is
460 dependent on the tissue-specific expression of *PLS* (Liu et al., 2010) (Figure S13) and
461 is mediated through its interaction with the ethylene receptor.

462 Future structural studies should reveal more about the PLS-ETR1-RAN1-
463 chaperone interaction and diverse roles of copper ions in ethylene signal transduction,
464 which represents a new paradigm for the regulation of signaling protein function by
465 metals.

466

467

468 # METHODS

469 **Plant Material**

470 Seedlings of *Arabidopsis thaliana* ecotype either C24 or Col-0, or *pls* mutants or
471 transgenic *PLS* overexpressers, all from lab stocks, were grown on solid sterile half-
472 strength MS10 medium on 2.5% Phytagel (Sigma-Aldrich) in 90 mm Petri dishes
473 (Sarstedt, Leicester, UK) at 21°C, under a 16 hour photoperiod as described (Casson
474 et al., 2002; Chilley et al., 2006). *Nicotiana benthamiana* plants (lab stocks) were grown
475 in a controlled environment (21°C, 16 h photoperiod) for transient expression studies in
476 leaf tissue. For hydroponic feeding studies, *Arabidopsis* seedlings were cultured in liquid
477 medium (1 ml/well) in sterile 24-well plates (Sarstedt), essentially as described
478 (Matsuzaki et al., 2010). For hormone and peptide assays, one seedling was grown in
479 each well, at 21°C, under a 16 h photoperiod. For peptide feeding experiments, purified
480 freeze-dried peptide was dissolved in DMSO to create a 500 µM stock solution. Peptide
481 stock solution was added to liquid ½ MS10 plant media containing 0.1% DMSO to make
482 a final peptide concentration of 50 or 100 nM (or 10, 25, 50 and 100 nM for dose-
483 dependent assays). For copper treatments, 1 mM $CuSO_4$ solution was filter-sterilized
484 and added to autoclaved liquid ½ MS10 plant media to create final $CuSO_4$
485 concentrations of 0, 5, 10, 15, 20, 25, 30, 35, 40, 45 and 50 µM. The copper chelator
486 bathocuproine disulphonic acid (BCS) was added to liquid medium to produce final
487 concentrations of 0, 10, 50, 100, 250 and 500 µM. Seedlings were scanned to create a
488 digital image and root lengths of seedlings were measured using ImageJ. Statistical
489 analysis was performed using the Real Statistics Resource Pack software (Release 3.8,
490 www.real-statistics.com) in Excel (Microsoft).

491

492 **Peptide Synthesis**

493 Peptides were either obtained from Cambridge Research Biochemicals (Billingham, UK)
494 or synthesized in the laboratory by Fmoc solid phase peptide synthesis (SPPS) on a
495 CEM Liberty1 single-channel peptide synthesiser equipped with a Discover microwave
496 unit. Reactions were performed in a 30 ml PTFE reaction vessel with microwave heating
497 FW: EpiLife Media and agitation by bubbling nitrogen. Peptide synthesis was carried out
498 using 2-chlorotrityl chloride resin (0.122 mmol g^{-1}, Novabiochem) using Fmoc-protected
499 amino acids. The first amino acid residue at the C-terminus (histidine) was coupled

500 manually by mixing 76 mg (1 eq.) Fmoc-His(Trt)-OH, 0.09 ml (4 eq.) *N,N*-
501 diisopropylethylamine (DIPEA), 1 ml dichloromethane (DCM) and 1 ml
502 dimethylformamide (DMF) until the amino acid powder had dissolved. The mixture was
503 added to 0.1 mmol resin and stirred gently for 120 min at room temperature. Resin was
504 washed with 3x DCM/MeOH/DIPEA (17:2:1), 3x DCM, 2x DMF and 2x DCM. Amino acid
505 coupling reactions were performed using Fmoc-protected amino acids present in a 5-
506 fold excess (2 M concentration), HOBt (0.5 M HOBt in DMF, used at the activator
507 position) and DIC (0.8 M in DMSO, used at the activator base position). For double and
508 triple couplings the reaction vessel was drained after each coupling cycle and fresh
509 reagents were added. Before each coupling, a room temperature preactivation period
510 of 1 to 2 h was used. Microwave-assisted couplings were performed for 10 min at 75°C
511 at 25W power. Cys and His residues were coupled at low temperature (10 min at room
512 temperature followed by 10 min at 50°C, 25W). Arg residues were double coupled, firstly
513 by 45 minutes at room temperature plus 5 minutes at 75°C (25W), and second by the
514 standard microwave conditions above. Fmoc group removal was carried out by two
515 piperidine solution treatments (20% piperidine in DMF) in succession: 5 minutes then
516 10 minutes. Peptide cleavage from resin was carried out in 3 ml 95% TFA in dH_2O/TIPS
517 (2.85 ml TFA, 0.15 ml dH_2O, 0.15 ml triisopropylsilane). Peptide was dissolved in water
518 with a small volume of MeCN and lyophilized to produce a powder using a Christ ALPHA
519 1-2 LD_{plus} freeze dryer.
520
521 **Preparative High-Performance Liquid Chromatography (HPLC)**
522 Peptide products were analysed and purified by HPLC at 280 nm. 25-50 mg of freeze-
523 dried peptide sample was dissolved in 1 ml 1:1 H_2O:MeCN and injected onto a Speck
524 and Burke Analytical C18 Column (5.0 µm, 10.0 x 250 mm) attached to a PerkinElmer
525 (Massachusetts, USA) Series 200 LC Pump and 785A UV/Vis Detector. Separation was
526 achieved by gradient elution of 10-80% solvent B (solvent A = 0.08% TFA in water;
527 solvent B = 0.08% TFA in ACN) over 60 min, followed by 80-100% B over 10 min, with
528 a flow rate of 2 ml/min. Selected peptide fractions were lyophilized and a mass assigned
529 using MALDI-TOF MS. Peptide sequences were identified using MALDI-TOF MS, using
530 an Autoflex II ToF/ToF mass spectrometer (Bruker Daltonik GmBH, Germany) equipped

531 with a 337 nm nitrogen laser. MS data was processed using FlexAnalysis 2.0 (Bruker
532 Daltonik GmBH).
533
534 **Imaging**
535 CSLM images for propidium iodide and GFP were obtained by a Leica SP5 TCS
536 confocal microscope as previously described (Rowe et al., 2016). *pPLS::PLS:GFP,*
537 *pPLS::GFP* and *p35S::GFP* seedlings were grown for 7 d on Phytagel ½ MS10 medium
538 before ca. 25 mm of the root tip was removed and mounted in dH_2O prior to imaging.
539 The ER marker *p35S::RFP:HDEL* (*24*) (provided by Dr. Pengwei Wang, Durham
540 University), and the trans-Golgi apparatus marker *pFGC-ST:mCherry* (from Nottingham
541 Arabidopsis Stock Centre, www.arabidopsis.info) were introduced into *pPLS::PLS:GFP*
542 plants by the floral dip method of transformation (Clough and Bent, 1998) using *A.*
543 *tumefaciens* GV3 101. ER was also localized using ER Tracker™ Red (Thermofisher).
544 Seven day-old seedlings were stained for 30 min in the dark in liquid ½ MS10 media
545 containing 1 μM ER Tracker™ Red.
546
547 **RNA Isolation, RNA Sequencing, RT-qPCR**
548 RNA was extracted from 7 day-old seedlings grown on half strength MS10 medium
549 essentially as described (Thompson et al., 2023). The Illumina HiSeq 2500 System was
550 used for RNA sequencing of three biological replicate samples, with libraries prepared using the
551 Illumina TruSeq Stranded Total RNA with Ribo-Zero Plant Sample Preparation kit (RS-122-
552 2401), essentially as described (Thompson et al., 2023). Library quality control was carried out
553 again using a TapeStation with D1000 ScreenTape (catalog number 5067-5582). RNA-seq data
554 were aligned to the TAIR10 (EnsemblePlants, release 58) genome sequence with
555 corresponding gtf file using STAR (v 2.7.11a; Dobin et al., 2013) to obtain read count per gene.
556 Read count per gene was analysed using DESeq2 v 1.40.2 (Love et al., 2014) to get p values,
557 adjusted p values, and log2 fold changes. Differentially expressed genes (DEGs) were identified
558 with the criteria of adjusted p value < 0.05. Gene ontology analysis was performed using AgriGO
559 (Tian et al., 2017) singular enrichment analysis. Gene expression heatmaps were generated
560 from log2 normalized counts using pheatmap (v1.0.12, https://cran.r-
561 project.org/web/packages/pheatmap/index.html) with row scaling. RNA-seq data were
562 deposited in GEO (https://www.ncbi.nlm.nih.gov/geo/) with accession number GSE256166
563 (Mudge et al., 2024).

564 For RT-qPCR, RNA was extracted from 7 day-old seedlings (3 biological
565 replicates, 20 mg of tissue) as described (Thompson et al., 2023). Samples were
566 checked for the presence of genomic DNA by PCR with *ACTIN2* primers ACT2 forward
567 and reverse. Primer sequences were determined using Primer-BLAST
568 (https://www.ncbi.nlm.nih.gov/tools/primer-blast/). Primers are listed in Table S7.
569
570 **Protein-protein interaction studies**
571 **Yeast 2-hybrid**
572 The GAL4 two-hybrid phagemid vector system was used to detect protein-protein
573 interactions *in vivo* in yeast, using the reporter genes β-galactosidase *(lacZ)* and
574 histidine (*HIS3*) in the YRG-2 yeast strain, essentially as described (Zhong et al., 2008**)**.
575 DNA that encodes the target (ETR1) and bait (PLS) was inserted into the pAD-GAL4-
576 2.1 A and pBD-GAL4 Cam phagemid vectors respectively and expressed as hybrid
577 protein. The hybrid proteins were then assayed for protein-protein interaction.
578 DNA encoding the target and bait proteins were prepared by PCR amplification
579 using primer designed the specifically for the DNA encoding the target (ETR1) and bait
580 (PLS). Each set of primer contained specific endonucleases on the ends of primer
581 corresponding to the endonucleases in the MCS of pAD-GAL4-2.1 A and pBD-GAL4
582 Cam phagemid vectors. The DNA construct of the target (ETR1) and bait (PLS) with
583 specific restriction sites on the ends was then transformed into the TOPO 2.1 vector to
584 check the sequence of the amplified DNA by sequencing with M13 forward (CTG GCC
585 GTC GTT TTA C) and M13 reverse (CAG GAA ACA GCT ATG AC). The two vectors,
586 pAD-GAL4-2.1 and pBD-GAL4 Cam were digested using specific restriction
587 endonucleases and dephosphorylated prior to ligating the insert DNA. The DNA
588 encoding the target (ETR1) and bait (PLS) was then ligated into the same reading frame
589 as the GAL4 AD of the pAD-GAL4-2.1 phagemid vector and the GAL4 BD of the pBD-
590 GAL4 Cam phagemid vector.
591 The following primers were used for PCR amplification:
592 ETR1:
593 Forward primer GAA TCC ATG GAA GTC TGC AAT TGT A (Eco RI on 5’ end)
594 Reverse primer GTC GAC TTA CAT GCC CTC GTA CA (Sal I on 5’end)
595 PLS:

596 Forward primer CTG GAG ATG AAA CCC AGA CTT TGT (Xho I on 5' end)
597 Reverse primer GTC GAC ATG GAT TTT AAA AAG TTT (Sal I on 5' end)
598 The pGAL4 control plasmid was used alone to verify that induction of the *lacZ*
599 and *HIS3* genes has occurred and that the gene products are detectable in the assay
600 used. The pLamin C control plasmid was used in pairwise combination with the pAD-
601 WT control plasmid or with the pAD-MUT control plasmid to verify that the *lacZ* and *HIS3*
602 genes are not induced as the protein expressed by each of these pairs do not interact
603 *in vivo*.
604 Control plasmids were transformed into the YRG-2 strain prior to the initial
605 transformation of the bait and the target plasmids and used separately or in pairwise
606 combination in the transformation of the YRG-2 yeast strain. Yeast competent cells were
607 cotransformed with the bait and target plasmids by sequential transformation.
608
609 **Gene cloning for co-immunoprecipitation**
610 To investigate the interaction between the PLS peptide and the ethylene receptor ETR1,
611 two DNA constructs were created by Gateway cloning. The 105-nucleotide *PLS* gene
612 (without the stop codon) was inserted into the pEarlyGate103 (pEG103) destination
613 vector, containing the *p35S* promoter and a C-terminal GFP tag, producing a vector
614 containing the *p35S::PLS:GFP* DNA. The ETR1 cDNA was inserted into the
615 pEarlyGate301 (pEG301) vector to create a *p35S::ETR1:HA* construct, producing an
616 ETR1 protein with a C-terminal HA tag.
617
618 **Infiltration into *Nicotiana benthamiana***
619 The transient expression of constructs in *Nicotiana benthamiana* (tobacco) leaves was
620 as previously described (Voinnet et al., 2007). Experiments were replicated up to 5
621 times. Competent *Agrobacterium tumefaciens* GV3101 cells were transformed with the
622 desired plasmid containing the gene of interest and each injected with a syringe. The
623 plants were approximately 7 to 10 weeks old; the chosen leaves were healthy and of
624 length 3-6 cm, and 3 to 4 leaves were infiltrated with each construct.
625

626 **Protein extraction and PLS/ETR1 co-immunoprecipitation**

627 Total protein was extracted from the infiltrated leaves of *N. benthamiana* plants 3 d after
628 infiltration for co-immunoprecipitation experiments to investigate the interaction between
629 PLS and ETR1 proteins, essentially as described previously (Srivastava et al., 2020).
630 For competition assays, 5 nM or 25 nM full-length PLS peptide was also infiltrated in the
631 presence of 50 μM MG-132 (a proteasome inhibitor) 30 min prior to tissue freezing.
632 ChromoTek (Planegg, Germany) anti-GFP beads were used to immunoprecipitate the PLS-GFP
633 protein, and Sigma-Aldrich (St. Louis, USA) anti-HA beads for the HA-tagged ETR1.

634 SDS-PAGE was used to separate protein fragments. The complexed proteins
635 from the pull-down assay were analysed on 10-12% acrylamide gels. Membranes were
636 incubated with primary antibody for 2.5 h (GFP, Abcam, Cambridge, UK: rabbit,
637 1:10000; HA (Roche), rat, 1:3000; Rubisco large subunit (Agrisera), rabbit, 1:10000).
638 Excess primary antibody was then removed by washing three times in 2x TBST (150
639 mM NaCl, 10 mM Tris, 0.1% (v/v) Tween 20, pH 7.4) for 2 m, 5 min and 10 min, and
640 subsequently incubated for 1 h with the ECL peroxidase-labelled anti-rabbit or anti-rat
641 IgG secondary antibody, diluted 1:20000 in TBST. Excess secondary antibody was
642 removed again by washing three times in 1x TBST, as with the primary antibody. In
643 order to visualize the probed blot, the membrane was incubated with ECL Western
644 Blotting Detection Reagent immediately prior to imaging. The horseradish peroxidase
645 conjugated to the secondary antibody was detected by using X-ray film.

646

647 **Estimation of synthetic PLS concentration**

648 Freeze-dried synthetic PLS peptide (Cambridge Research Biochemicals, Billingham)
649 was dissolved in DMSO. An aliquot was added to aqueous buffer (10 mM HEPES pH7,
650 20 mM NaCl, 80 mM KCl) and absorbance at 280 nm was recorded. Concentration was
651 estimated from the absorbance and the ProtParam estimated extinction coefficient of
652 2,980 M^{-1} cm^{-1}. Concurrent with this a sample was submitted for quantitative amino acid
653 analysis (Abingdon Health Laboratory Services). From this analysis a conversion factor
654 of 2.27 was generated, which was applied to concentrations determined by A280 nm.

655

656

657

658 **ATX1 purification**

659 *E. coli* BL21(DE3) containing pETatx1 was used to overexpress the wild type *ATX1* gene
660 from *Arabidopsis thaliana* (optimised for expression in *E. coli*, Novoprolabs). Harvested
661 cells were collected and frozen at -20 ^{o}C overnight then defrosted, resuspended in 20
662 mM HEPES (pH 7.0), 10 mM EDTA, 100 mM NaCl, 10 mM DTT. Cells were sonicated
663 (Bandelin Sonoplus), supernatant separated by size exclusion chromatography (GE
664 Healthcare, HiLoad 26.600 Superdex 75 pg) metal-free buffer lacking EDTA. Fractions
665 containing ATX1 were incubated overnight and pooled before transfer into an anaerobic
666 chamber (Belle Technology) via desalting column where reductant was removed. ATX1
667 was quantified by combination of Bradford assay and Ellman's reagent to ensure the
668 fully reduced state of the protein. Samples were also analysed for metal content by ICP-
669 MS to ensure > 95% apo-ATX1.

670

671 **MBP-PLS/mutant purification**

672 A fusion of PLS to MBP was created using the NEBExpress MBP Fusion and Purification
673 System. Two complementary oligonucleotide primers encoding PLS (optimised for
674 expression in *E. coli*) were annealed and inserted into the pMal-c5x plasmid at XmnI
675 and SalI insertion sites.

676 The three mutants MBP-PLS(C6S), MBP-PLS(C17S) and MBP-
677 PLS(C6S/C17S) were created by site-directed mutagenesis (QuikChange II, Agilent). *E.*
678 *coli* NEB Express containing the pMal plasmid with the correct MBP-PLS mutant was
679 used to overexpress each protein. Harvested cells were resuspended in 20 mM Tris-
680 HCl (pH 7.4), 200 mM NaCl, 1 mM EDTA and frozen at -20 ^{o}C overnight. Cells were
681 defrosted in cold H_2O, sonicated, purified by ammonium sulphate precipitation (where
682 MBP-PLS precipitates >60% saturation), separated on MBP-trap (GE Healthcare) and
683 eluted using buffer containing 10 mM maltose. MBP-PLS-containing fractions were
684 pooled and concentrated using centrifugal concentrator (Corning, Spin-X UF 30 KDa)
685 and buffer exchanged by desalting column into metal-free 20 mM HEPES (pH 7.0), 50
686 mM NaCl buffer in an anaerobic chamber (Belle Technology). Mutants containing thiols
687 were quantified Ellman's assay and MBP-PLS(C6S/C17S), which lacks all thiols, was
688 quantified by Bradford assay alone. Samples were also analysed for metal content by
689 ICP-MS to ensure >95% apo-protein.

690

691 **Anaerobic spectroscopic analysis of Cu(I) complexes**

692 All Cu(I) titration experiments were carried out in an anaerobic chamber (Belle
693 Technology) using metal-free CHELEX-treated, degassed buffers. For experiments
694 titrating Cu(I), aqueous $CuSO_4$ stock was quantified in advance by ICP-MS and diluted
695 to working concentrations. The reductant NH_2OH was included at final concentration of
696 1 mM to retain Cu(I) in its reduced state. Proteins were diluted in buffer to the final
697 concentration specified in each titration in air-tight quartz cuvettes (Helma), and after
698 addition of probe to the concentration specified, titrated with $CuSO_4$. After each addition,
699 solutions were thoroughly mixed and absorbance spectra recorded using a Lambda 35
700 UV/Vis spectrophotometer (Perkin Elmer). Titration isotherm data was fitted using
701 simulated affinity curves using DynaFit (Kuzmič, 2009).

702

703 **Interaction studies of PLS with copper transporter ETR1 by Microscale**
704 **Thermophoresis**

705 Fluorescently labelled ETR1 truncation mutants were added to a dilution series of PLS
706 in 50 mM HEPES, 150 mM NaCl, 0.015 % (wv) FosCholine 16 (pH 7.6) or 50 mM Tris,
707 300 mM NaCl, 0.015 % (w/v) FosCholine 16 (pH 7.6). Dissociation constants were
708 calculated using GraphPad Prism 5.

709

710 **Determination of dissociation constants for the PLS-ETR1 interaction**

711 Full-length ETR1 and truncation mutants were purified and labelled as described in
712 (Milić et al., 2018). 94 µM PLS were diluted serially in 50 mM Tris and 300 mM NaCl (pH
713 7.6). Fluorescently labelled receptor was added at a final concentration of 50 nM.
714 Thermophoretic behaviour was measured in premium capillaries at 50 % LED and 50 %
715 MST power. In case of a binding event, data were fitted using GraphPad Prism 5.

716

717 **Interaction studies of PLS with copper transporter RAN1 and copper chaperones**
718 **by microscale thermophoresis**

719 PLS was titrated to fluorescently labelled RAN1 and RAN1 truncation mutants. RAN1,
720 NterRAN1 and CterRAN1 were purified and labelled as described (Hoppen et al., 2019).
721 NterRAN1 is a truncation containing only of two N-terminal metal-binding-domains,

722 whereas CterRAN1 is a construct lacking this region. Direct interaction between PLS
723 and RAN1 was observed using Microscale Thermophoresis. Dissociation constants
724 were determined using GraphPad Prism 5. Titration experiments were also carried out
725 with fluorescently labelled copper chaperones ATX, CCH and CCHΔ, a mutant lacking
726 the plant specific C-terminal extension. Proteins were purified and labelled as described
727 (Hoppen et al., 2019).
728
729 **Ratiometric analysis of roGFP2 fusion proteins**
730 N- and C-terminal roGFP2 fusion proteins of PLS were generated by Gateway cloning.
731 Infiltration and transient expression of roGFP2 fusions and control proteins were carried
732 out as described (Brach et al., 2009). Image acquisition and data analysis were carried
733 out as described by Hoppen et al. (2019). A minimum of 10 leaf optical sections were
734 imaged and used for ratiometric analysis of the redox sensitive excitation properties of
735 roGFP2.
736
737 **SUPPLEMENTAL INFORMATION**
738 All study data are included in the article and/or Supplemental Information are available
739 at *Molecular Plant Online*. RNA-seq and root assay data are available at GEO
740 accession GSE256166:
741 https://eur01.safelinks.protection.outlook.com/?url=https%3A%2F%2Fwww.ncbi.nlm.ni
742 h.gov%2Fgeo%2Fquery%2Facc.cgi%3Facc%3DGSE256166&data=05%7C02%7Ckei
743 th.lindsey%40durham.ac.uk%7C9637f7022a2240cfb10608dc324244cd%7C7250d88b
744 4b684529be44d59a2d8a6f94%7C0%7C0%7C638440507397042151%7CUnknown%
745 7CTWFpbGZsb3d8eyJWIjoiMC4wLjAwMDAiLCJQIjoiV2luMzIiLCJBTiI6Ik1haWwiLCJ
746 XVCI6Mn0%3D%7C0%7C%7C%7C&sdata=U4JHCoviYbdEbF76Tws8Ridq7W%2B5
747 Hq2qBVN%2BFjIysgw%3D&reserved=0
748
749 **FUNDING**
750 The authors acknowledge financial support from: UK Biotechnology and Biological
751 Sciences Research Council BB/E006531/1, BBS/B/0773X, BB/J014516/1 (KL),
752 BB/V006002/1, BB/M011186/1 (NJR); Deutsche Forschungsgemeinschaft (German
753 Research Foundation) 267205415 – SFB 1208 project B06 (GG).

754

755 **AUTHOR CONTRIBUTIONS**

756 KL and NJR initiated the project. KL, JFT, NJR, AS and GG designed and supervised
757 aspects of the project. AJM, SM, WM, BO-P, WS, WW, CT, DR, FMH, CH and BU
758 carried out the experimental work and prepared the Figures. KL, NJR and GG drafted
759 the early version of the manuscript, and all authors reviewed and edited the manuscript.

760

761 **ACKNOWLEDGEMENTS**

762 Authors declare no competing interests. We thank Prof. Steven Cobb (Durham
763 University Department of Chemistry) for advice on peptide synthesis, and Dr. Andrew
764 Foster (Durham University Department of Chemistry) for preliminary peptide-Cu
765 interaction analysis.

766

767 **DECLARATION OF INTERESTS**

768 The authors declare no competing interests.

769

770 ## REFERENCES

771 **Abel, S., Nguyen, M., Chow, W., and Theologis, A**. (1995). *ASC4*, a primary
772 indoleacetic acid-responsive gene encoding 1-amino-cyclopropane-1-carboxylate
773 synthase in *Arabidopsis thaliana*. J. Biol. Chem. **270**: 19093–19099.

774 **Andrés-Colás, N., Sancenón, V., Rodríguez-Navarro, S., Mayo, S., Thiele, D.J.,**
775 **Ecker, J.R., Puig, S., and Peñarrubia, L**. (2006). The Arabidopsis heavy metal
776 P-type ATPase HMA5 interacts with metallochaperones and functions in copper
777 detoxification of roots. Plant J. **45**: 225–236.

778 **Bauer, M. and Papenbrock, J.** (2002). Identification and characterization of single-
779 domain thiosulfate sulfurtransferases from *Arabidopsis thaliana*. FEBS Lett. **532**:
780 427-431.

781 **Binder, B.M., Rodriguez, F.I., and Bleecker, A.B.** (2010). The copper transporter
782 RAN1 is essential for biogenesis of ethylene receptors in Arabidopsis. J. Biol.
783 Chem. **285**: 37263-37270.

784 **Bishopp, A., Help, H., El-Showk, S., Weijers, D., Scheres, B., Friml, J., Benkova,**
785 **E., Mahonen, A.P., and Helariutta, Y.** (2011). A mutually inhibitory interaction

786 between auxin and cytokinin specifies vascular pattern in roots. Curr. Biol. **21**: 917-
787 926.
788 **Brach, T., Soyk, S Müller, C., Hinz, G., Hell, R., Brandizzi, F., and Meyer, A.J.**
789 (2009). Non-invasive topology of membrane proteins in the secretory pathway.
790 Plant J. 57: 534-541.
791 **Burkhead, J.L., Reynolds, K.A., Abdel-Ghany, S.E., Cohu, C.M., and Pilon, M**.
792 (2009). Copper homeostasis. New Phytol. **182**: 799–816.
793 **Campos, M. L., de Souza, C. M. de Oliviera, K.B.S., Dias, S.C., and Franco, O.L.**
794 (2018). The role of antimicrobial peptides in plant immunity. J. Exp. Bot. **69**: 4997-
795 5011.
796 **Capraro, J., Sessa, F., Magni, C., Scarafoni, A., Maffioloi, E., Tedeschi, G., Croy,**
797 **R.D.D., and Duranti, M.** (2015). Proteolytic cleavage at twin arginine residues
798 affects structural and functional transitions of Lupin seed 11S storage globulin.
799 PLOS ONE **10**: e0117406.
800 **Casareno, R.L., Waggoner, D., and Gitlin, J.D.** (1998). The copper chaperone CCS
801 directly interacts with copper/zinc superoxide dismutase. J. Biol. Chem. **273**:
802 23625–23628.
803 **Casson, S.A., Chilley, P.M., Topping, J.F., Evans, I.M., Souter, M.A., and Lindsey,**
804 **K.** (2002). The *POLARIS* gene of Arabidopsis encodes a predicted peptide
805 required for correct root growth and leaf vascular patterning. Plant Cell **14**: 1705-
806 1721.
807 **Chang, C.R.** (2003). Ethylene signaling: the MAPK module has finally landed. Trends
808 Plant Sci. **8**: 365-368.
809 **Chang, C., Kwok, S.F., Bleecker, A.B., and Meyerowitz, E.M.** (1993). Arabidopsis
810 ethylene-response gene *ETR1* - similarity of product to 2-component regulators.
811 Science **262**: 539-544.
812 **Chen, G., Li, J., Han, H., Du, R., and Wang, X.** (2022). Physiological and molecular
813 mechanisms of plant responses to copper stress. Int. J. Mol. Sci. **23**: 12950.
814 **Chen, Y.F., Randlett, M.D., Findell, J.L., and Schaller, G.E.** (2002). Localization of
815 the ethylene receptor ETR1 to the endoplasmic reticulum of Arabidopsis. J. Biol.
816 Chem. **277**: 19861-19866.

817 **Chilley, P.M., Casson, S.A., Tarkowski, P., Hawkins, N., Wang, K.L., Hussey, P.J.,**
818 **Beale, M., Ecker, J.R., Sandberg, G.K., and Lindsey, K.** (2006). The POLARIS
819 peptide of Arabidopsis regulates auxin transport and root growth via effects on
820 ethylene signaling. Plant Cell **18**: 3058-3072.
821 **Chu, C.C., Lee, W.C., Guo, W.Y., Pan, S.M., Li, L.J., Chen, H.M., and Jinn, T.L.**
822 (2005). A copper chaperone for superoxide dismutase that confers three types of
823 copper/zinc superoxide dismutase activity in Arabidopsis. Plant Physiol. **139**: 425–
824 436.
825 **Clough, S.J., and Bent A.F.** (1998). Floral dip: a simplified method for *Agrobacterium*-
826 mediated transformation of *Arabidopsis thaliana*. Plant J. **6**: 735-743.
827 **Dobin, A., Davis, C.A., Schlesinger, F., Drenkow, J., Zaleski, C., Jha, S., Batut, P.,**
828 **Chaisson, M., and Gingeras, T.R.** (2013). STAR: ultrafast universal RNA-seq
829 aligner. Bioinformatics **29**: 15-21.
830 **Duckert, P., Brunak, S., and Blom, N.** (2004). Prediction of preprotein convertase
831 cleavage sites. Prot. Engin. Design Select. **17**: 107-112.
832 **Gao, Z.Y., Chen, Y.-F., Randlett, M.D., Zhao, X.-C., Findell, J.L., Kieber, J.J., and**
833 **Schaller, G.E.** (2003). Localization of the Raf-like kinase CTR1 to the endoplasmic
834 reticulum of Arabidopsis through participation in ethylene receptor signaling
835 complexes. J. Biol. Chem. **278**: 34725-34732.
836 **Grefen, C., Staedele, K., Ruzicka, K., Obrdlik, P., Harter, K., and Horak, J.** (2008).
837 Subcellular localization and *in vivo* interactions of the *Arabidopsis thaliana*
838 ethylene receptor family members. Molec. Plant **1**: 308-320.
839 **Hall, A.E., Findell, J.L., Schaller, G.E., Sisler, E.C., and Bleecker, A.B.** (2000).
840 Ethylene perception by the ERS1 protein in Arabidopsis. Plant Physiol. **123**: 1449-
841 1457.
842 **Hirayama, T., Kieber, J.J., Hirayama, N., Kogan, M., Guzman, P., Nourizadek, S.,**
843 **Alonso, J.M., Dailey, W.P. Dancis, A. and Ecker, J.R.** (1999). RESPONSIVE-
844 TO-ANTAGONIST1, a Menkes/Wilson disease-related copper transporter, is
845 required for ethylene signaling in Arabidopsis. Cell **97**: 383-393.
846 **Hoppen, C., Müller, L.S., Hänsch, B. Uzun, D., Milic, A.J., Meyer, Weidtkamp-**
847 **Peters, S., and Groth G.**, (2019). Soluble and membrane-bound protein carrier
848 mediate direct copper transport to the ethylene receptor family. Sci Rep. **9**: 10715.

849 **Hua, J., Chang, C., Sun, Q., and Meyerowitz, E.M.** (1995). Ethylene insensitivity
850 conferred by Arabidopsis *ERS* gene. Science **269**: 1712-1714.
851 **Hua, J., Sakai, H., Nourizadeh, S., Chen, Q.G., Bleecker, A.B., Ecker, J.R., and**
852 **Meyerowitz, E.M.** (1998). EIN4 and ERS2 are members of the putative ethylene
853 receptor gene family in Arabidopsis. Plant Cell **10**: 1321-1332.
854 **Johnson, P.R., and Ecker, J.R.** (1998). The ethylene gas signal transduction pathway:
855 A molecular perspective. Ann. Rev. Genet. **32**: 227-254.
856 **Kim, J.S., Jeon, B.W., and Kim, J.** (2021). Signaling peptides regulating abiotic
857 stresses in plants. Front. Plant Sci. **12**: 704490.
858 **Kuzmič, P.** (2009). DynaFit—a software package for enzymology. Meth. Enzymol. **467**:
859 247–280.
860 **Lee, H., Sparkes, I., Gattolin, S., Dzimitrowicz, N., Roberts, L.M., Hawes, C., and**
861 **Frigerio, L.** (2013). An Arabidopsis reticulon and the atlastin homologue *RHD3-*
862 *like2* act together in shaping the tubular endoplasmic reticulum. New Phytol. **197**:
863 481-489.
864 **Li, W., Lacey, R.F., Ye, Y., Lu, J., Yeh, K.-C., Xiao, Y., Li, L., Wen, C.-K., Binder,**
865 **B.M., and Zhao, Y.** (2017). Triplin, a small molecule, reveals copper ion transport
866 in ethylene signaling from ATX1 to RAN1. PLOS Genet. **13**: e1006703.
867 **Liu, J. Mehdi, S. Topping, J. Tarkowski, P. and Lindsey, K.** (2010). Modelling and
868 experimental analysis of hormonal crosstalk in Arabidopsis. Molec. Systems Biol.
869 **6**: 373.
870 **Liu, J. Mehdi, S. Topping, J. Friml, J. and Lindsey, K.** (2013). Interaction of PLS and
871 PIN and hormonal crosstalk in Arabidopsis root development. Front. Plant Sci. **4**:
872 75.
873 **Love, M.I., Huber, W., and Anders, S.** (2014). Moderated estimation of fold change
874 and dispersion for RNA-seq data with DESeq2. Genome Biol. **15**: 550.
875 **Matsuzaki, Y. Ogawa-Ohnishi, M. Mori, A. and Matsubayashi, Y.** (2010). Secreted
876 peptide signals required for maintenance of root stem cell niche in Arabidopsis.
877 Science **329**: 1065-1067.
878 **McDaniel, B.K., and Binder, B.M.** (2012). ETHYLENE RECEPTOR 1 (ETR1) is
879 sufficient and has the predominant role in mediating inhibition of ethylene
880 responses by silver in *Arabidopsis thaliana*. J. Biol. Chem. **287**: 26094-26103.

881 **Milić, D. Dick, M. Mulnaes, D. Pfleger, C. Kinnen, A. Gohlke, H., and Groth, G**.
882 (2018). Recognition motif and mechanism of ripening inhibitory peptides in plant
883 hormone receptor ETR1. Sci. Rep. **8**: 1–12.
884 **Moore, S., Zhang, X., Mudge, A., Rowe, J.H., Topping, J.F., Liu, J., and Lindsey, K.**
885 (2015). Spatiotemporal modelling of hormonal crosstalk explains the level and
886 patterning of hormones and gene expression in *Arabidopsis thaliana* wildtype and
887 mutant roots. New Phytol. **207**: 1110-1122.
888 **Morgan, M.T., Bourassa, D., Harankhedkar, S., McCallum, A.M., Zlatic, S.A., Calvo,**
889 **J.S., Meloni, G., Faundez, V., and Fahrni, C.J.** (2019). Ratiometric two-photon
890 microscopy reveals attomolar copper buffering in normal and Menkes mutant cells.
891 Proc. Natl. Acad. Sci. USA **116**: 12167–12172.
892 **Mudge, A.J., Mehdi, S., Michaels, W., Orosa-Puente, B., W. Shen, Wei, W.,**
893 **Tomlinson, C., Sadanandom, A., Hetherington, F.M., C. Hoppen, Uzun, B.,**
894 **Groth, G., Topping, J.F., Robinson, N.J., and Lindsey, K.** (2024). Data from: A
895 peptide that regulates metalation and function of the *Arabidopsis* ethylene
896 receptor. GEO accession
897 GSE256166: https://eur01.safelinks.protection.outlook.com/?url=https%3A%2F
898 %2Fwww.ncbi.nlm.nih.gov%2Fgeo%2Fquery%2Facc.cgi%3Facc%3DGSE25616
899 6&data=05%7C02%7Ckeith.lindsey%40durham.ac.uk%7C9637f7022a2240cfb10
900 608dc324244cd%7C7250d88b4b684529be44d59a2d8a6f94%7C0%7C0%7C63
901 8440507397042151%7CUnknown%7CTWFpbGZsb3d8eyJWIjoiMC4wLjAwMDAi
902 LCJQIjoiV2luMzIiLCJBTiI6Ik1haWwiLCJXVCI6Mn0%3D%7C0%7C%7C%7C&sd
903 ata=U4JHCoviYbdEbF76Tws8Ridq7W%2B5Hq2qBVN%2BFjIysgw%3D&reserve
904 d=0
905 **Olsson, V., Joos, L., Zhu, S., Gevaert, K., Butenko, M., and De Smet, I.** (2019). Look
906 closely, the beautiful may be small: Precursor-derived peptides in plants. Ann. Rev.
907 Plant Biol. **70**: 153-186.
908 **Ortega-Martinez, O., Pernas, M., Carol, R.J., and Dolan, L.** (2007). Ethylene
909 modulates stem cell division in the *Arabidopsis thaliana* root. Science **317**: 507-
910 510.
911 **Puig, S., Mira, H., Dorcey, E., Sancenón, V., Andrés-Colás, N., Garcia-Molina, A.,**
912 **Burkhead, J.L., Gogolin, K.A., Abdel-Ghany, S.E., Thiele, D.J., Ecker, J.R.,**

913 **Pilon, M., and Penarrubia, L.** (2007). Higher plants possess two different types
914 of ATX1-like copper chaperones. Biochem. Biophys. Res. Commun. **354**: 385–
915 390.
916 **Qu, X., Hall, B.P., Gao, Z.Y., and Schaller, G.E.** (2007). A strong constitutive ethylene-
917 response phenotype conferred on Arabidopsis plants containing null mutations in
918 the ethylene receptors *ETR1* and *ERS1*. BMC Plant Biol. **7**: 3.
919 **Robinson, N.J.. and Winge, D.R.** (2010). Copper metallochaperones. Ann. Rev.
920 Biochem. **79**: 537-562.
921 **Rodriguez, F.I., Esch, J.J., Hall, A.E., Binder, B.M., Schaller, G.E., and Bleecker,**
922 **A.B.** (1999). A copper cofactor for the ethylene receptor ETR1 from Arabidopsis.
923 Science **283**: 996-998.
924 **Rowe, J.H., Topping, J.F., Liu, J., and Lindsey, K.** (2016). Abscisic acid regulates
925 root growth under osmotic stress conditions via an interacting hormonal network
926 with cytokinin, ethylene and auxin. New Phytol. **211**: 225-239.
927 **Sabatini, S., Beis, D., Wolkenfelt, H., Murfett, J., Guilfoyle, T., Malamy, J., Benfey,**
928 **P., Leyser, O., Bechtold, N., Weisbeek, P., and Scheres, B.** (1999). An auxin-
929 dependent distal organizer of pattern and polarity in the Arabidopsis root. Cell **99**:
930 463-472.
931 **Sakai, H., Hua, J., Chen, Q.G., Chang, C., Medrano, L.J., Bleecker, A.B., and**
932 **Meyerowitz, E.M.** (1998). *ETR2* is an *ETR1*-like gene involved in ethylene
933 signaling in *Arabidopsis*. Proc. Natl. Acad. Sci. USA **95**: 5812-5817.
934 **Schaller, G.E., Ladd, A.N., Lanahan, M.B., Spanbauer, J.M., and Bleecker, A.B.**
935 (1995). The ethylene response mediator ETR1 from Arabidopsis forms a disulfide-
936 linked dimer. J. Biol. Chem. **270**: 12526-12530.
937 **Schott-Verdugo, S. Müller, L. Classen, E. Gohlke, H., and Groth, G**. (2019).
938 Structural model of the ETR1 ethylene receptor transmembrane sensor domain.
939 Sci. Rep. **9**: 8869.
940 **Shin, L.-J., Lo, J.-C., and Yeh, K.-C**. (2012). Copper chaperone antioxidant protein1 is
941 essential for copper homeostasis. Plant Physiol. **159**: 1099-1110.
942 **Srivastava, M., Srivastava, A.J., Orosa-Puente, B., Campanaro, A., Zhang, C., and**
943 **Sadanandom, A.** (2020). SUMO conjugaiton to BZR1 enables brassinosteroid

944 signaling to integrate environbmental cues to shape plant growth. Curr. Biol. **30**:
945 1410-1423.
946 **Thompson, H.L., Shen, W., Matus, R., Kakkar, M., Jones, C., Dolan, D., Grellscheid,**
947 **S., Yang, X., Zhang, N., Mozaffari-Jovin, S. Chen, C. Zhang, X. Topping, J.F.**
948 **and Lindsey, K.** (2023). MERISTEM-DEFECTIVE regulates the balance between
949 stemness and differentiation in the root meristem through RNA splicing control.
950 Development **150**: dev201476.
951 **Tian, T., Liu, Y., Yan, H., You, Q., Yi, X., Du, Z., Xu, W., and Su, Z.** (2017). agriGO
952 v2.0: a GO analysis toolkit from the agricultural community, 2017 update. Nucl.
953 Acids Res. **45**: W122-W129.
954 **Yu, C.H., Yang, N., Bothe, J., Tonelli, M., Nokhrin, S., Dolgova, N.V., Braiterman,**
955 **L., Lutsenko, S., and Dmitriev, O.Y.** (2017). The metal chaperone Atox1
956 regulates the activity of the human copper transporter ATP7B by modulating
957 domain dynamics. J. Biol. Chem. **292**: 18169.
958 **Voinnet, O., Rivas, S., Mestre, P., and Baulcombe, D.** (2003). An enhanced transient
959 expression system in plants based on suppression of gene silencing by the p19
960 protein of tomato bushy stunt virus. Plant J. **33**: 949-956.
961 **Williams, L.E., and Mills, R.F.** (2005). P(1B)-ATPases: an ancient family of transition
962 metal pumps with diverse functions in plants. Trends Plant Sci. **10**: 491–502.
963 **Willoughby, A.C., and Nimchuk, Z.L.** (2021). WOX going on: CLE peptides in plant
964 development. Curr. Opin. Plant Biol. **63**: 102056.
965 **Xiao, Z., Brose, J., Schimo, S., Ackland, S.M., La Fontaine, S., and Wedd, A.G.**
966 (2011). Unification of the copper(I) binding affinities of the metallo-chaperones
967 Atx1, Atox1, and related proteins: detection probes and affinity standards. J. Biol.
968 Chem. **286**: 11047-11055.
969 **Woeste, K.E., and Kieber, J.J.** (2000). A strong loss-of-function mutation in RAN1
970 results in constitutive activation of the ethylene response pathway as well as a
971 rosette-lethal phenotype. Plant Cell **12**: 443-455.
972 **Zhong, S., Lin, Z., and Grierson, D.** (2008). Tomato ethylene receptor-CTR
973 interactions: visualization of NEVER-RIPE interactions with multiple CTRs at the
974 endoplasmic reticulum. J. Exp. Bot. **59**: 965-972.
975

976

977 **Figure Legends**

978

979 **Figure 1. The PLS peptide is required for ethylene control of seedling growth, is**
980 **structurally and functionally conserved, and complements the *Arabidopsis pls***
981 **mutant.**

982 (**A**). Amino acid sequence of the PLS peptide from *Arabidopsis thaliana* with *Camelina*
983 *sativa* PLS sequence (*C.s*), and synthetic truncations N1, N2, C1 and C2, indicated by
984 horizontal lines. Two cysteine residues are highlighted in bold. (**B**) Wild type (left) and
985 *pls* mutant (right); bar = 5 mm. (**C**) Expression levels of 24 ethylene-responsive genes
986 in *pls* and *PLS* overexpressing (PLSox) seedlings, compared to wild type levels. Data
987 are expressed as $\log_2$-fold changes in *pls* mutant and PLSox seedlings compared wild
988 type with respective significance levels (*P-adj* value) provided in Table S1. A $P < 0.05$
989 and $\log_2$-fold of change of ± 0.5 was chosen to identify differentially expressed genes.
990 (**D**) Effect of *Arabidopsis* PLS full length peptide, *A.t.* PLS(FL), and *Camelina* PLS
991 peptide (*C.s.* PLS) on *Arabidopsis* primary root length. Wild type (C24; blue bars) and
992 *pls* mutant seedlings (red bars) were grown hydroponically in the presence (100 nM) or
993 absence of peptide for 10 d. ***: $P < 0.05$, *t*-test between C24 and *pls*, n = 20-25. (**E**)
994 Effect of PLS full length and truncated peptides on wild type (blue bars) and *pls* mutant
995 (red bars) *Arabidopsis* primary root length. Seedlings were grown hydroponically in the
996 presence of 50 nM peptide for 10 d. C1 = C-terminal 14 amino acids, C2 = C-terminal
997 24 amino acids, N1 = N-terminal 22 amino acids, N2 = N-terminal 9 amino acids, full
998 length PLS = 36 amino acids. Error bars show ± 1 standard error, n = 25. ***: $P < 0.05$,
999 *t*-test between C24 and *pls*, n = 25.

1000

1001 **Figure 2. PLS localizes to the endoplasmic reticulum.**

1002 (**A-O**) PLS::PLS:GFP fusion protein (**A, G, J**) colocalizes with endoplasmic reticulum
1003 markers ER Tracker (**B, C, C inset**) and RFP:HDEL (**H, I, I inset**), but free GFP does
1004 not (**D-F**, **M-O**). PLS:GFP staining is seen also in nuclei (n). PLS::PLS:GFP (**J**) does not
1005 co-localize with the *trans*-Golgi markers ST-mCherry SH:GFP (**K, L**). Scale bars = 25
1006 µm (**C, I**), 10 µm (**F, I, O**). Root epidermal cells in the transition zone were imaged. (**p**)
1007 Ratiometric analysis of roGFP2 fusion constructs transiently expressed in *N.*
1008 *benthamiana*. Comparison of excitation ratios of PLS-roGFP2 and roGFP2-PLS with

1009 control constructs (free roGFP, SEC22 fusions) reveals that PLS localizes to the
1010 cytosolic side of the ER.
1011
1012 **Figure 3. PLS interacts with the ethylene receptor ETR1.**
1013 (**A**) Co-immunoprecipitation of PLS:GFP by ETR1:HA (upper panel) in leaves of
1014 *Nicotiana benthamiana*, in the presence and absence of 0.5 μM $CuSO_4$ and EDTA (to
1015 remove Cu). Lower panels show presence of ETR1:HA in extracts using anti-HA
1016 antibody, and protein input blots using anti-GFP and anti-Rubisco. (**B**) Densitometric
1017 scan of immunoblot. (**C**) Competition assay showing a reduced binding between
1018 PLS:GFP and ETR1:HA in the presence of 0, 5 nM or 25 nM PLS peptide, in the
1019 presence of 0.5 μM $CuSO_4$ and 50 μM MG-132, a proteasome inhibitor (upper panel).
1020 Lower panel shows ETR1:HA in extracts using anti-HA antibody. (**D**) Densitometric scan
1021 of immunoblot. (**E**) Co-immunopreciptation of ETR1:HA (upper panel) in leaves of *N.*
1022 *benthamiana*, showing the effect of EDTA (to remove Cu) on interaction between
1023 ETR1:HA and PLS:GFP. Lower panels shows presence of ETR1:HA in extracts using
1024 anti-HA antibody, and protein input blots using anti-ETR1-HA and anti-Rubisco. (**F**)
1025 Densitometric scan of immunoblot. α-GFP, anti-GFP antibody; α-HA, anti-HA antibody.
1026 (**G**) Microscale thermophoresis binding curves of different ETR1 truncations with PLS.
1027 Binding of PLS was observed with full-length ETR1 and all C-terminal truncations but
1028 not with $ETR1^{306-738}$ lacking the N-terminal transmembrane part of the receptor.
1029
1030 **Figure 4. PLS binds copper and interacts with RAN1 and copper chaperones.**
1031 (**A**) C6S and C17S in PLS are required for function. Seedlings were grown
1032 hydroponically for 10 d in the presence (100 nM) or absence of peptide (FL or C6S,
1033 C17S). Blue bars are C24, red bars are *pls*. *: P <0.05, *t*-test between C24 and *pls*, n =
1034 25. Error bars show ± 1 standard error, n = 14-22. (**B**) BCA absorbance in the presence
1035 of synthetic PLS (44.8 μM, filled symbols) or an equivalent volume (to PLS) of DMSO
1036 (open symbols). Experiments with PLS used 88.3 μM (circles), 84 μM (triangles) and
1037 88.4 μM (squares) BCA. The control experiment with DMSO used 85.3 μM BCA. (**C**)
1038 UV-vis apo subtracted difference spectra of synthetic PLS (19.8 μM) upon titration with
1039 CuCl (top left); binding isotherm of the feature at 242 nm (top right). Fluorescence
1040 spectra of PLS (19.8 μM) upon titration with CuCl (bottom left); binding isotherm of the

1041 feature at 306 nm (bottom right). (**D**) Absorption of BCA (17.3 μM) titrated with Cu(I)
1042 (representative spectrum, n = 2, full data in Fig. S6). (**E**) Binding isotherms ($A_{358\ nm}$) of
1043 BCA (10 μM) in the presence/absence (filled/empty symbols, respectively) of 14 μM
1044 MBP-PLS (circles) or MBP-PLS mutants (C6S, C17S and C6S/C17S: triangles,
1045 diamonds and squares respectively) titrated with Cu(I) (n = 3, ± SD). Arrow indicates ca.
1046 7 μM withholding of Cu(I) from BCA. (**F**) Binding isotherms ($A_{358\ nm}$) of BCA (50 μM) in
1047 the presence/absence of 10 μM MBP-PLS (filled/empty symbols, respectively) titrated
1048 with Cu(I). Model (solid line) describes Cu(I)-binding as a 2:1 complex, with β_2 affinity of
1049 3.79 (± 1.5) x10^{19} M^{-2}. Dotted lines simulate 10x weaker or tighter affinity (n = 3, ± SD).
1050 (**G**) Simulated Cu(I) occupancy (Supplementary Text) as a function of [PLS] using β_2
1051 Cu(I) affinity of 3.79 x10^{19} M^{-2}. Inset, *Arabidopsis* ATX1 (20 μM, filled circles) withholds
1052 one Cu(I) equivalent from 20 μM BCA (open circles, BCA-alone) (n = 3, ±SD), with K_D
1053 Cu(I) 5.47 x10^{-18} M (Fig. S3). (**H**) Microscale thermophoresis binding curves of copper
1054 transporter RAN1 with PLS. (**I**) Microscale thermophoresis binding curves of soluble
1055 copper chaperones ATX1 and CCH with PLS (n = 3, ± SD).
1056
1057 **Figure 5. Possible models of the role of PLS in ethylene signalling.**
1058 In these models, we make the assumption that RAN1 and ETR1 are in the same
1059 membranous compartment (likely the ER) at least transiently. RAN1 is believed to pump
1060 Cu(I) into the ER lumen, and then to ETR1. In air (absence of ethylene; top left), the
1061 receptor complex is active and activates CTR1, which is a nregative regulator of
1062 ethylene responses. In the presence of ethylene (top right), the receptor is in an inactive
1063 state, cannot activate CTR1, resulting in ethylene responses. In Model 1, RAN1 pumps
1064 Cu(I) into the ER lumen, and then PLS transfers Cu(I) from RAN1 to ETR1. In Model 2,
1065 PLS removes Cu(I) from ETR1, and lack of Cu(I) in ETR1 (as in *ran1* LOF mutants)
1066 leads to inactive ETR1, inactive CTR1 and constitutive ethylene signalling. In Model 3,
1067 PLS binds to ETR1 (with binding potentially enhanced by the Cu(I) in the ETR1
1068 transmembrane domain) and affects the receptor conformation, potentially blocking
1069 ethylene binding to ETR1 or inducing some other conformational change, leading to
1070 active ETR1, active CTR1 and reduced ethylene signalling. Model 3 is consistent with
1071 the observed *pls* loss of function mutant showing enhanced ethylene responses. Drawn
1072 using Biorender.

1073

A MKPRLCFNSRRRSISPCYISIS *C.s*

MKPRLCFNFRRRSISPCYISISYLLVAKLFKLFKIH *A.t*

N2 N1 C1 C2

B

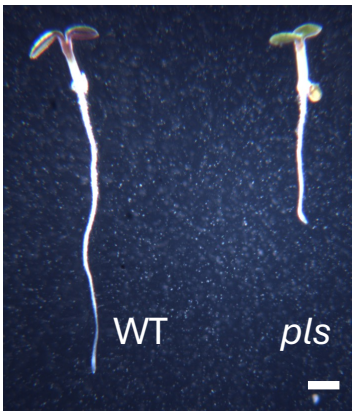

C

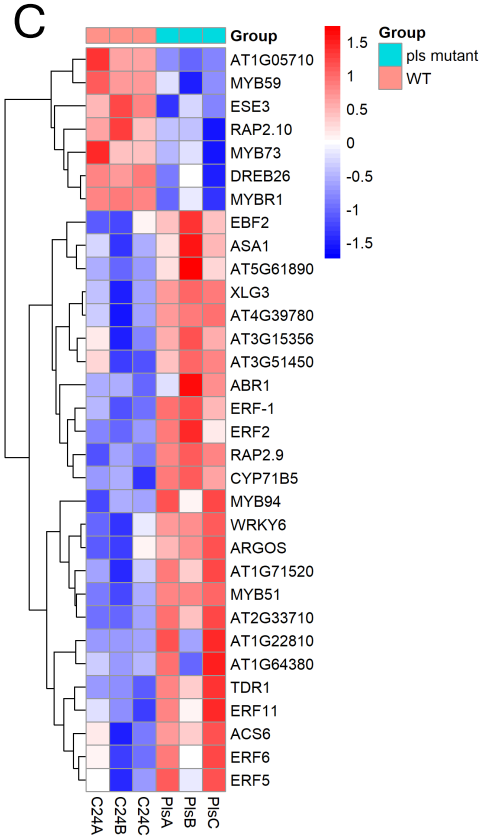

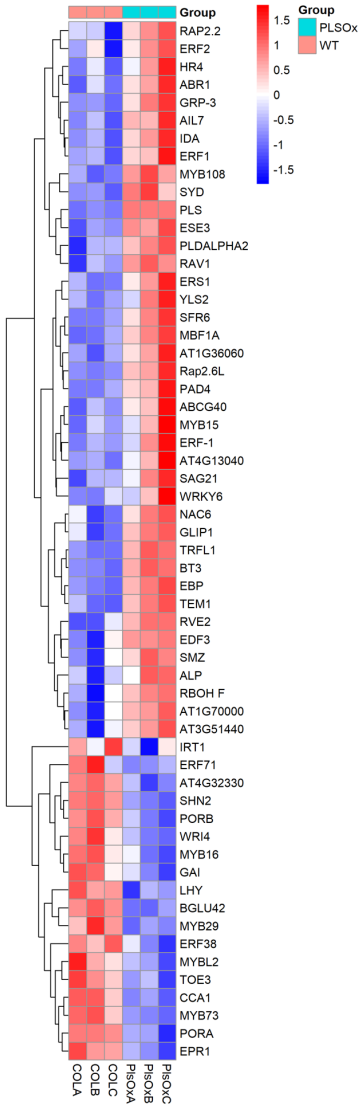

D

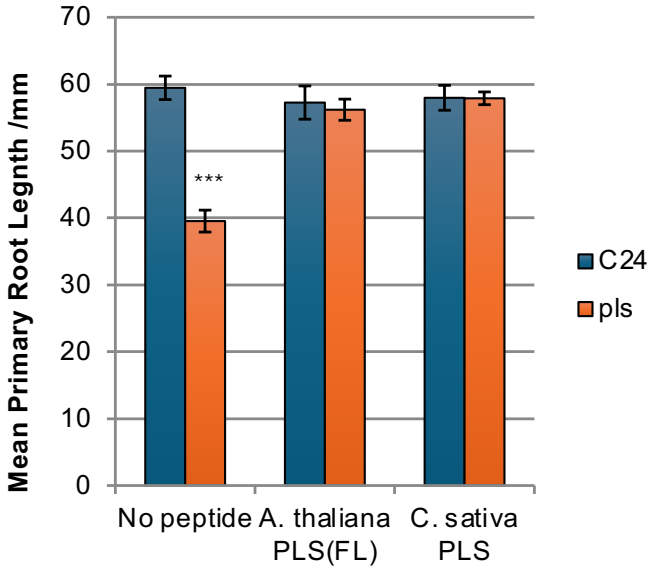

E

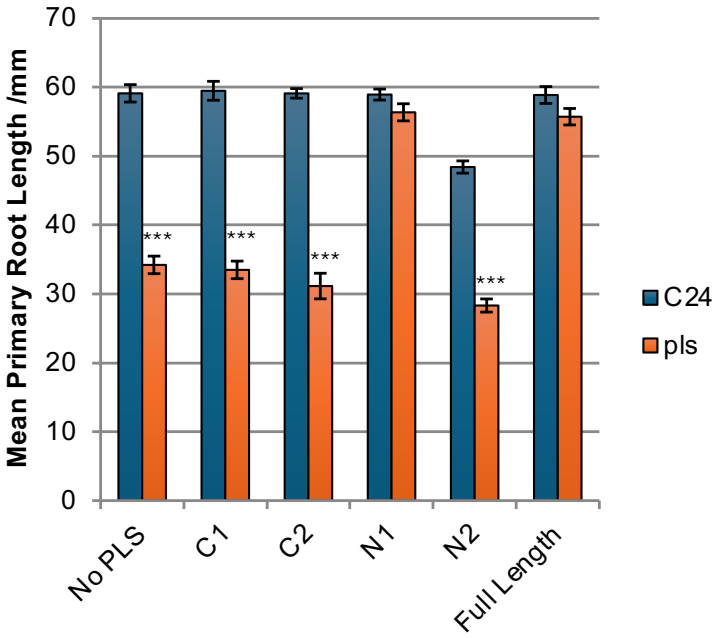

Fig. 1

Figure 1. The PLS peptide is required for ethylene control of seedling growth, is structurally and functionally conserved, and complements the *Arabidopsis pls* mutant.

(**A**). Amino acid sequence of the PLS peptide from *Arabidopsis thaliana* (*A.t*) with *Camelina sativa* PLS sequence (*C.s*), and synthetic truncations N1, N2, C1 and C2, indicated by horizontal lines. Two cysteine residues are highlighted in bold. (**B**) Wild type (left) and *pls* mutant (right); bar = 5 mm. (**C**) Heat maps showing expression levels of 32 ethylene-responsive genes in *pls* (left panel) and of 58 genes in *PLS* overexpressing (PLSox) seedlings (right panel), compared to wildtype levels. Data for 3 biological replicates are shown, and are expressed as $\log_2$-fold changes in *pls* mutant and PLSox seedlings compared wildtype with respective significance levels (*P-adj* value) provided in Tables S1 and S2. A $P < 0.05$ and $\log_2$-fold of change of $\pm$ 0.5 was chosen to identify differentially expressed genes. (**D**) Effect of *Arabidopsis* PLS full length peptide, *A.t.* PLS(FL), and *Camelina* PLS peptide (*C.s.* PLS) on *Arabidopsis* primary root length. Wildtype (C24; blue bars) and *pls* mutant seedlings (red bars) were grown hydroponically in the presence (100 nM) or absence of peptide for 10 d. ***: $P < 0.05$, *t*-test between C24 and *pls*, n = 20-25. (**E**) Effect of PLS full length and truncated peptides on wild type (blue bars) and *pls* mutant (red bars) *Arabidopsis* primary root length. Seedlings were grown hydroponically in the presence of 50 nM peptide for 10 d. C1 = C-terminal 14 amino acids, C2 = C-terminal 24 amino acids, N1 = N-terminal 22 amino acids, N2 = N-terminal 9 amino acids, full length PLS = 36 amino acids. Error bars show $\pm$ 1 standard error, n = 25. ***: $P < 0.05$, *t*-test between C24 and *pls*, n = 25.

Fig. 2

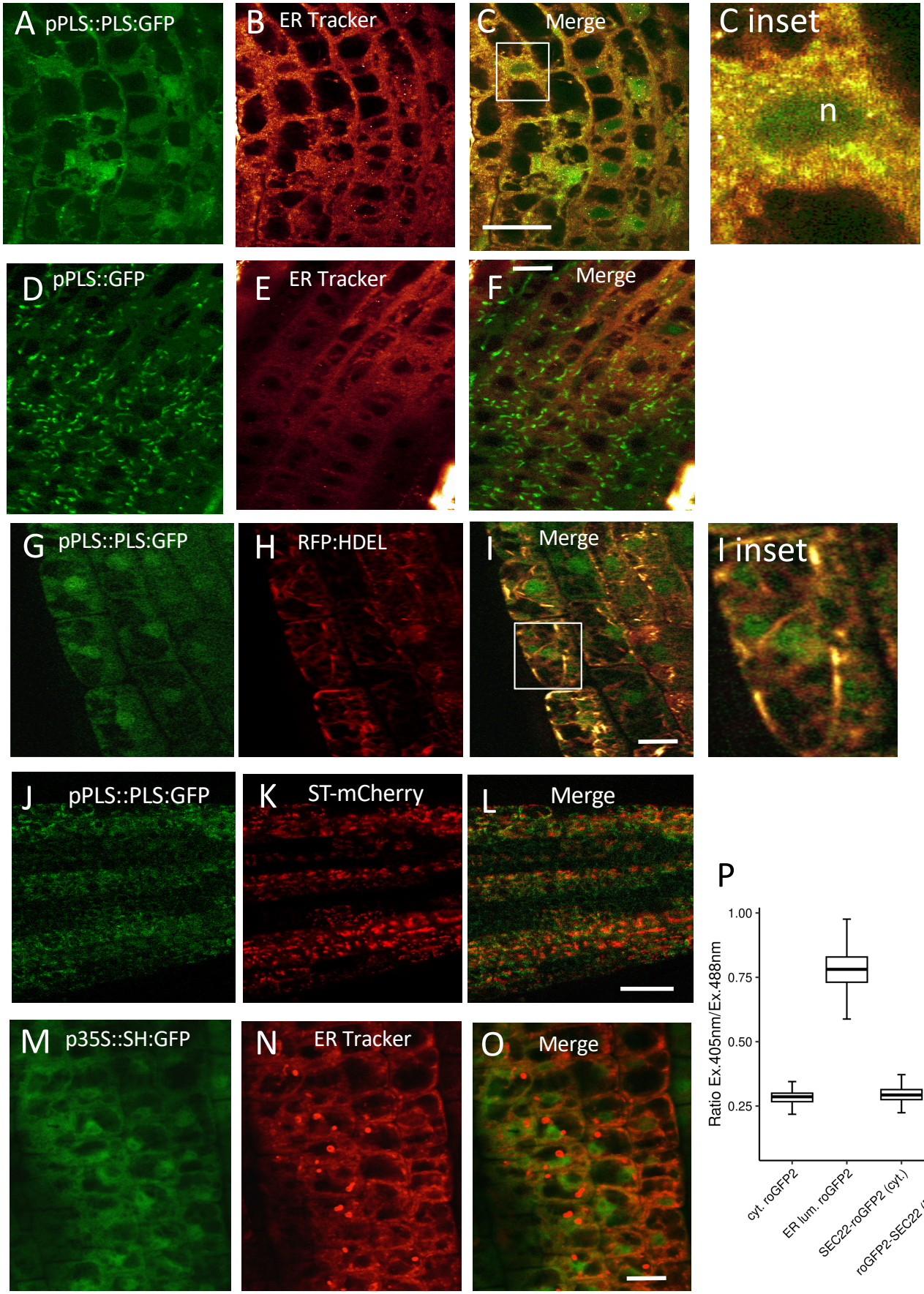
A pPLS::PLS:GFP
B ER Tracker
C Merge
C inset
n
D pPLS::GFP
E ER Tracker
F Merge
G pPLS::PLS:GFP
H RFP:HDEL
I Merge
I inset
J pPLS::PLS:GFP
K ST-mCherry
L Merge
M p35S::SH:GFP
N ER Tracker
O Merge

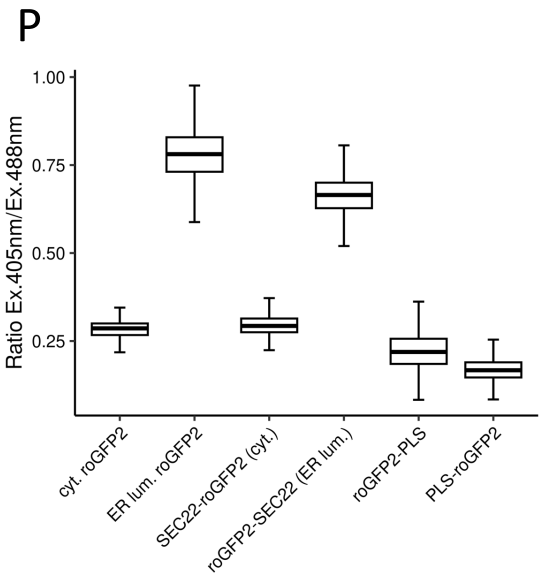
P
Ratio Ex.405nm/Ex.488nm
1.00
0.75
0.50
0.25
cyt. roGFP2
ER lum. roGFP2
SEC22-roGFP2 (cyt.)
roGFP2-SEC22 (ER lum.)
roGFP2-PLS
PLS-roGFP2

Figure 2. PLS localizes to the endoplasmic reticulum.
(**A-O**) PLS::PLS:GFP fusion protein (**A, G, J**) colocalizes with endoplasmic reticulum markers ER Tracker (**B, C, C inset**) and RFP:HDEL (**H, I, I inset**), but free GFP does not (**D-F**, **M-O**). PLS:GFP staining is seen also in nuclei (n). PLS::PLS:GFP (**J**) does not co-localize with the *trans*-Golgi markers ST-mCherry SH:GFP (**K, L**). Scale bars = 25 µm (**C, L**), 10 µm (**F, I, O**). Root epidermal cells in the transition zone were imaged. (**P**) Ratiometric analysis of roGFP2 fusion constructs transiently expressed in *N. benthamiana*. Comparison of excitation ratios of PLS-roGFP2 and roGFP2-PLS with control constructs (free roGFP, SEC22 fusions) reveals that PLS localizes to the cytosolic side of the ER.

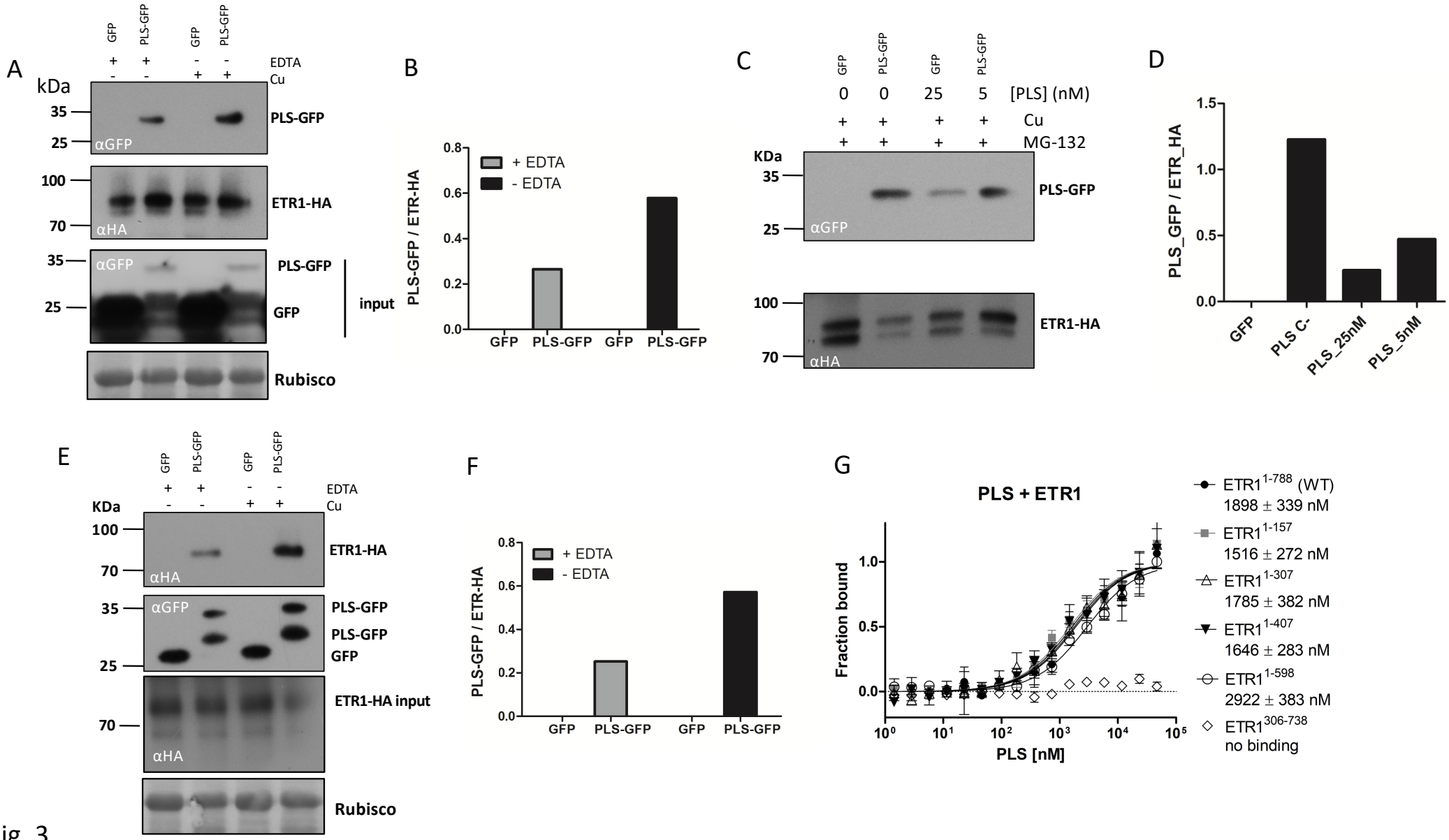
A
GFP
PLS-GFP
GFP
PLS-GFP
EDTA
Cu
kDa
35
25
αGFP
PLS-GFP
100
70
αHA
ETR1-HA
35
25
αGFP
PLS-GFP
GFP
input
Rubisco
B
PLS-GFP / ETR-HA
+ EDTA
- EDTA
GFP
PLS-GFP
GFP
PLS-GFP
C
GFP
PLS-GFP
GFP
PLS-GFP
0
0
25
5
[PLS] (nM)
Cu
MG-132
KDa
35
25
αGFP
PLS-GFP
100
70
αHA
ETR1-HA
D
PLS_GFP / ETR_HA
GFP
PLS C-
PLS_25nM
PLS_5nM
E
GFP
PLS-GFP
GFP
PLS-GFP
EDTA
Cu
KDa
100
70
αHA
ETR1-HA
35
25
αGFP
PLS-GFP
PLS-GFP
GFP
70
αHA
ETR1-HA input
Rubisco
F
PLS-GFP / ETR-HA
+ EDTA
- EDTA
GFP
PLS-GFP
GFP
PLS-GFP
G
PLS + ETR1
Fraction bound
PLS [nM]
ETR1 1-788 (WT)
1898 ± 339 nM
ETR1 1-157
1516 ± 272 nM
ETR1 1-307
1785 ± 382 nM
ETR1 1-407
1646 ± 283 nM
ETR1 1-598
2922 ± 383 nM
ETR1 306-738
no binding

Fig. 3

Figure 3. PLS interacts with the ethylene receptor ETR1.

(**A**) Co-immunoprecipitation of PLS:GFP by ETR1:HA (upper panel) in leaves of *Nicotiana benthamiana*, in the presence and absence of 0.5 μM $CuSO_4$ and EDTA (to remove Cu). Lower panels show presence of ETR1:HA in extracts using anti-HA antibody, and protein input blots using anti-GFP and anti-Rubisco. (**B**) Densitometric scan of immunoblot. (**C**) Competition assay showing a reduced binding between PLS:GFP and ETR1:HA in the presence of 0, 5 nM or 25 nM PLS peptide, in the presence of 0.5 μM $CuSO_4$ and 50 μM MG-132, a proteasome inhibitor (upper panel). Lower panel shows ETR1:HA in extracts using anti-HA antibody. (**D**) Densitometric scan of immunoblot. (**E**) Co-immunopreciptation of ETR1:HA (upper panel) in leaves of *N. benthamiana*, showing the effect of EDTA (to remove Cu) on interaction between ETR1:HA and PLS:GFP. Lower panels shows presence of ETR1:HA in extracts using anti-HA antibody, and protein input blots using anti-ETR1-HA and anti-Rubisco. (**F**) Densitometric scan of immunoblot. a-GFP, anti-GFP antibody; a-HA, anti-HA antibody. (**G**) Microscale thermophoresis binding curves of different ETR1 truncations with PLS. Binding of PLS was observed with full-length ETR1 and all C-terminal truncations but not with $ETR1^{306-738}$ lacking the N-terminal transmembrane part of the receptor.

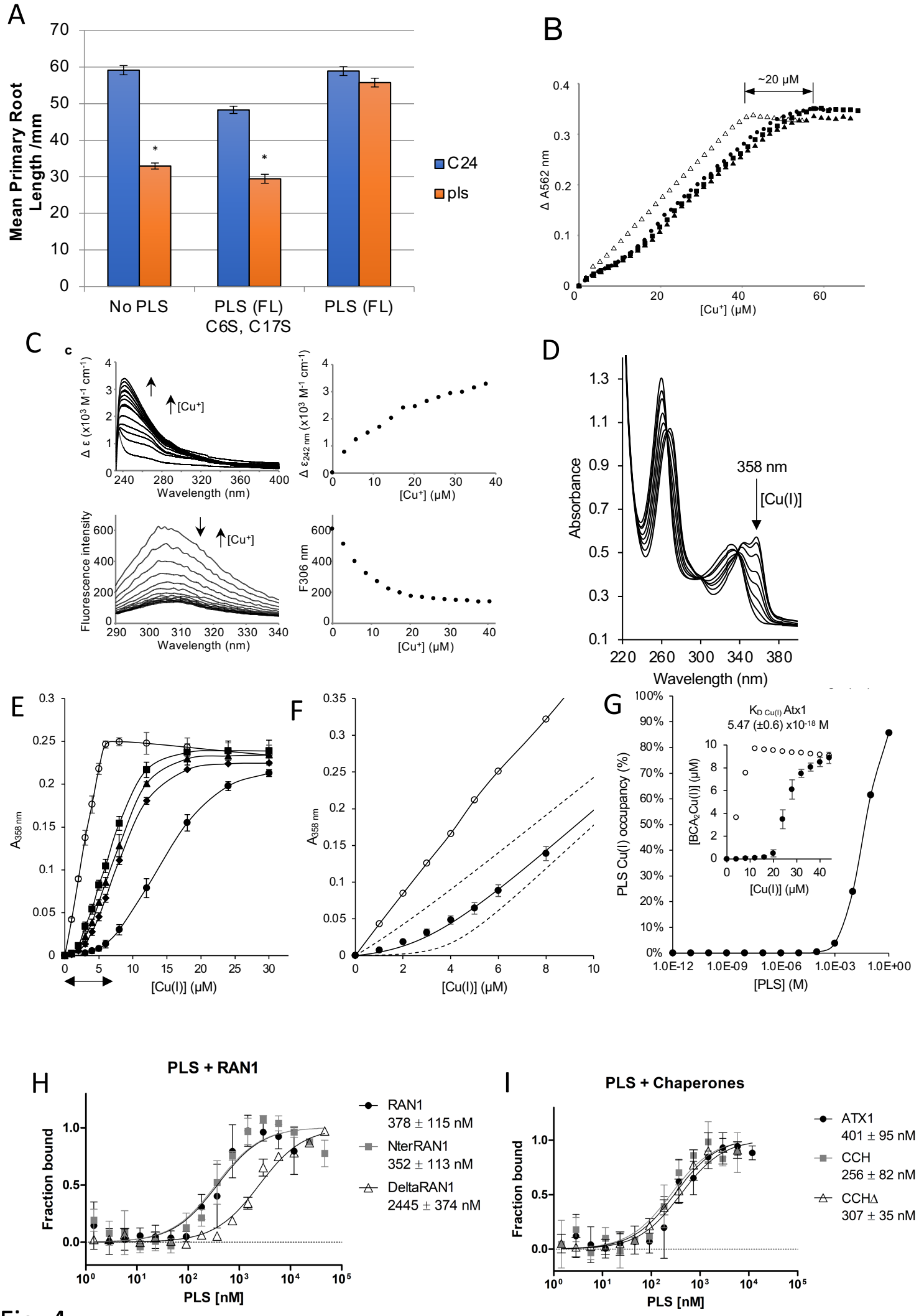
A
Mean Primary Root Length /mm
C24
pls
No PLS
PLS (FL)
PLS (FL) C6S, C17S
B
~20 µM
Δ A562 nm
[Cu+] (µM)
C
Δ ε (x10³ M⁻¹ cm⁻¹)
[Cu+]
Wavelength (nm)
Δ ε242 nm (x10³ M⁻¹ cm⁻¹)
Fluorescence intensity
F306 nm
D
Absorbance
358 nm
[Cu(I)]
Wavelength (nm)
E
A358 nm
[Cu(I)] (µM)
F
G
PLS Cu(I) occupancy (%)
[PLS] (M)
KD Cu(I) Atx1
5.47 (±0.6) x10-18 M
[BCA2Cu(I)] (µM)
H
PLS + RAN1
Fraction bound
PLS [nM]
RAN1
378 ± 115 nM
NterRAN1
352 ± 113 nM
DeltaRAN1
2445 ± 374 nM
I
PLS + Chaperones
ATX1
401 ± 95 nM
CCH
256 ± 82 nM
CCHΔ
307 ± 35 nM

Fig. 4

Figure 4. PLS binds copper and interacts with RAN1 and copper chaperones. (**A**) C6S and C17S in PLS are required for function. Seedlings were grown hydroponically for 10 d in the presence (100 nM) or absence of peptide (FL or C6S, C17S). Blue bars are C24, red bars are *pls*. * P <0.05, *t*-test between C24 and *pls*, n = 25. Error bars show ± 1 standard error, n = 14-22. (**B**) BCA absorbance in the presence of synthetic PLS (44.8 μM, filled symbols) or an equivalent volume (to PLS) of DMSO (open symbols). Experiments with PLS used 88.3 μM (circles), 84 μM (triangles) and 88.4 μM (squares) BCA. The control experiment with DMSO used 85.3 μM BCA. (**C**) UV-vis apo subtracted difference spectra of synthetic PLS (19.8 μM) upon titration with CuCl (top left); binding isotherm of the feature at 242 nm (top right). Fluorescence spectra of PLS (19.8 μM) upon titration with CuCl (bottom left); binding isotherm of the feature at 306 nm (bottom right). (**D**) Absorption of BCA (17.3 μM) titrated with Cu(I) (representative spectrum, n = 2, full data in Fig S6). (**E**) Binding isotherms ($A_{358\ nm}$) of BCA (10 μM) in the presence/absence (filled/empty symbols, respectively) of 14 μM MBP-PLS (circles) or MBP-PLS mutants (C6S, C17S and C6S/C17S: triangles, diamonds and squares respectively) titrated with Cu(I) (n = 3, ±SD). Arrow indicates ca. 7 μM withholding of Cu(I) from BCA. (**F**) Binding isotherms ($A_{358\ nm}$) of BCA (50 μM) in the presence/absence of 10 μM MBP-PLS (filled/empty symbols, respectively) titrated with Cu(I). Model (solid line) describes Cu(I)-binding as a 2:1 complex, with β_2 affinity of 3.79 (±1.5) x10^{19} M^{-2}. Dotted lines simulate 10x weaker or tighter affinity (n = 3, ±SD). (**G**) Simulated Cu(I) occupancy (Supplementary Text) as a function of [PLS] using β_2 Cu(I) affinity of 3.79 x10^{19} M^{-2}. Inset, *Arabidopsis* ATX1 (20 μM, filled circles) withholds one Cu(I) equivalent from 20 μM BCA (open circles, BCA-alone) (n = 3, ±SD), with K_D Cu(I) 5.47 x10^{-18} M (Fig. S3). (**H**) Microscale thermophoresis binding curves of copper transporter RAN1 with PLS. (**I**) Microscale thermophoresis binding curves of soluble copper chaperones ATX1 and CCH with PLS (n = 3, ±SD).

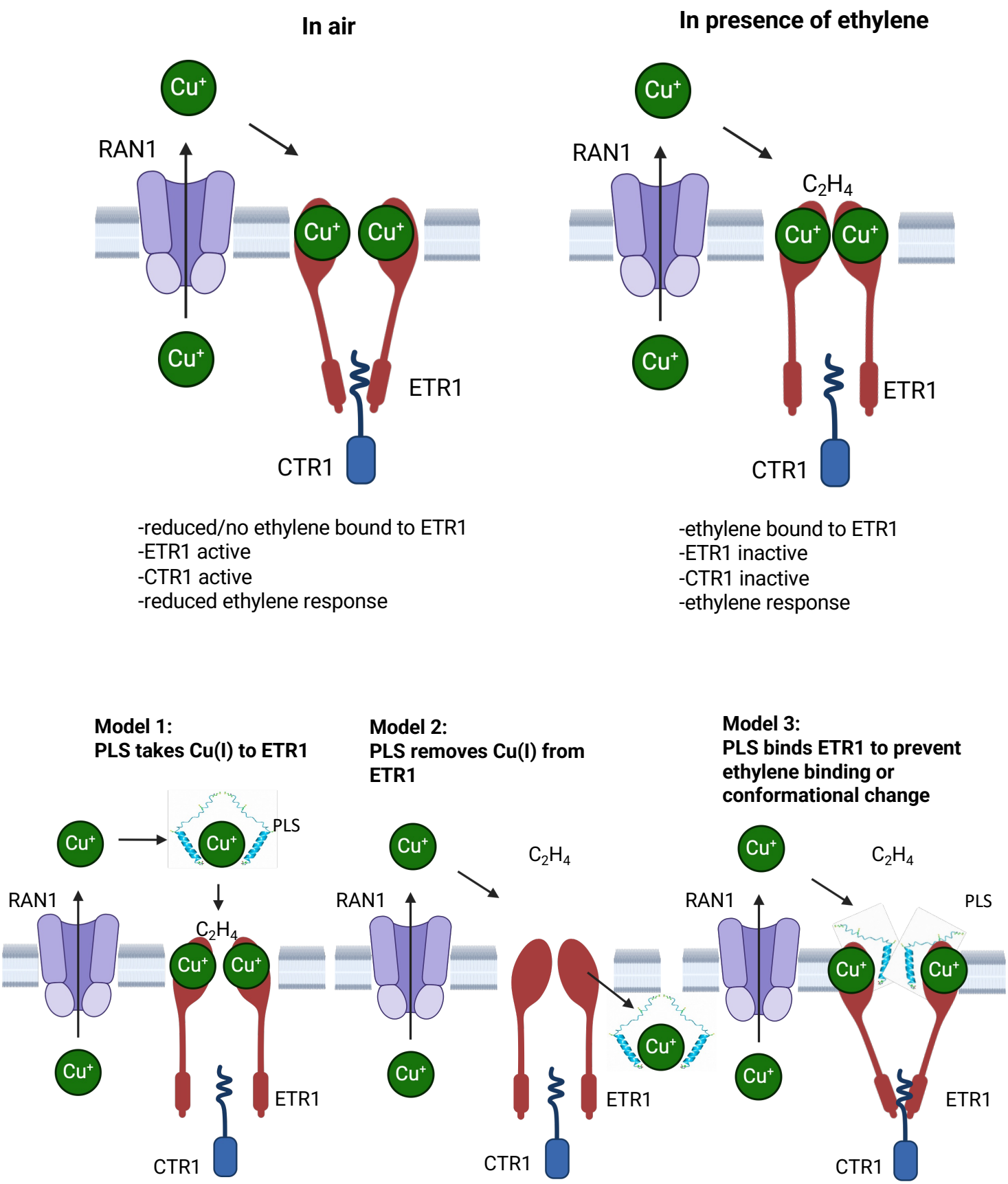
In air
In presence of ethylene
Cu+
RAN1
ETR1
CTR1
C2H4
-reduced/no ethylene bound to ETR1
-ETR1 active
-CTR1 active
-reduced ethylene response
-ethylene bound to ETR1
-ETR1 inactive
-CTR1 inactive
-ethylene response
Model 1:
PLS takes Cu(I) to ETR1
Model 2:
PLS removes Cu(I) from ETR1
Model 3:
PLS binds ETR1 to prevent ethylene binding or conformational change
PLS
-ethylene bound to ETR1
-ETR1 inactive
-CTR1 inactive
-ethylene response
-reduced Cu(I) bound to ETR1
-ETR1 inactive due to Cu-mediated conformational change
-CTR1 inactive
-constitutive ethylene response
-reduced/no ethylene bound to ETR1
-ETR1 active
-CTR1 active
-reduced ethylene response

Fig. 5

Figure 5. Possible models of the role of PLS in ethylene signalling.

In these models, we make the assumption that RAN1 and ETR1 are in the same membranous compartment (likely the ER) at least transiently. RAN1 is believed to pump Cu(I) into the ER lumen, and then to ETR1. In air (absence of ethylene; top left), the receptor complex is active and activates CTR1, which is a nregative regulator of ethylene responses. In the presence of ethylene (top right), the receptor is in an inactive state, cannot activate CTR1, resulting in ethylene responses. In Model 1, RAN1 pumps Cu(I) into the ER lumen, and then PLS transfers Cu(I) from RAN1 to ETR1. In Model 2, PLS removes Cu(I) from ETR1, and lack of Cu(I) in ETR1 (as in *ran1* LOF mutants) leads to inactive ETR1, inactive CTR1 and constitutive ethylene signalling. In Model 3, PLS binds to ETR1 (with binding potentially enhanced by the Cu(I) in the ETR1 transmembrane domain) and affects the receptor conformation, potentially blocking ethylene binding to ETR1 or inducing some other conformational change, leading to active ETR1, active CTR1 and reduced ethylene signalling. Model 3 is consistent with the observed *pls* loss of function mutant showing enhanced ethylene responses. Drawn using Biorender.